SENSOR-CRAFT ANALYTICAL CERTIFICATION

THESIS

Ronald W. Roberts, Jr., Captain, USAF

AFIT/GAE/ENY/03-6

DEPARTMENT OF THE AIR FORCE
AIR UNIVERSITY

AIR FORCE INSTITUTE OF TECHNOLOGY

Wright-Patterson Air Force Base, Ohio

AFIT/GAE/ENY/03-6

SENSOR-CRAFT ANALYTICAL CERTIFICATION

THESIS

Presented to the Faculty

Department of Aeronautics and Astronautics

Graduate School of Engineering and Management

Air Force Institute of Technology

Air University

Air Education and Training Command

In Partial Fulfillment of the Requirements for the

Degree of Master of Science in Aeronautical Engineering

Ronald W. Roberts, Jr., BS

Captain, USAF

March 2003

AFIT/GAE/ENY/03-6

SENSOR-CRAFT ANALYTICAL CERTIFICATION

Ronald W. Roberts, Jr., BS
Captain, USAF

Approved:

//Signed//	11 March, 2003
Robert A. Canfield (Chairman)	date
//Signed//	10 March, 2003
Anthony N. Palazotto (Member)	date
//Signed//	10 March, 2003
Curtis H. Spenny (Member)	date

Acknowledgments

I would like to express my sincere appreciation to my faculty advisor, Lt. Col. Robert A. Canfield, for his guidance and support throughout the course of this effort. I would, also, like to thank Dr. Maxwell Blair, from the Air Force Research Laboratory for the software support and perspective provided to me in this thesis. Finally, I extend heartfelt thanks to Jeremiah Allen for his software support. Without his assistance, this project would not have been completed.

Special thanks go to my wife for her patience, engineering sanity, grammatical skill and love.

Ronald W. Roberts, Jr.

Table of Contents

Page

List of Figures

Figure Page

List of Tables

List of Symbols

Symbol	Definition
a	Angle of Attack, Resizing Exponent
d	Aft-Wing Twist Angle
?	Air Density
e	Strain
s	Stress
?	Wing Sweep Angle
μ_g	Wing Mass Ratio
a	Slope of C_L – a
g	Acceleration Due to Gravity
c	Wing Chord Length
t	Element Thickness
x, y, z	Cartesian Coordinates
u, v, w	Displacements in Cartesian Coordinates
B	Derivative of Shape Function Matrix
C	Specific Fuel Consumption
D	Drag
K	Stiffness Matrix, Gust Alleviation Factor
L	Lift
R	Range

Symbol	Definition
S	Span, Wing Surface Area
V	Velocity, Volume
W	Weight
Xc.g.	Center of Gravity Location
Xa.c.	Aerodynamic Center Location

Abstract

This study developed a multi-disciplinary conceptual design of a joined-wing sensor-craft. Initial analysis was conducted using an aluminum model. Linear fully stressed design and flexible aerodynamic trim were used to converge to a minimum weight design that was aerodynamically stable. This optimized design was buckling safe. A similar optimization process using non-linear fully stressed design and flexible aerodynamic trim was conducted. The non-linear structural deformation was over ten times greater than the linear structural deformation. Again, the model was structurally and aerodynamically optimized. The linear optimization was repeated using a composite structural model incorporating Conformal Load-bearing Antenna Structures. This research demonstrated the importance of considering non-linearity and the coupling of aerodynamic and structural design.

SENSOR-CRAFT ANALYTICAL CERTIFICATION

I. Introduction

Overview

Sensor-craft is a conceptual unmanned air vehicle (UAV) based on an Air Force need for advanced, long-endurance tactical surveillance using current and future sensor technologies. The Air Force Research Laboratory, Air Vehicles Directorate, leads the sensor-craft conceptual design study.

A potential vehicle design is a joined-wing configuration that could lead to improved radar capabilities, increased aerodynamic performance, and structural weight savings. A typical joined-wing aircraft has a large lifting surface, named the aft-wing, connecting the top of the vertical tail structure to the main wing of the vehicle. The aft-wing is usually swept forward and down to attach the two structures (Fig. 1-1,1-2).

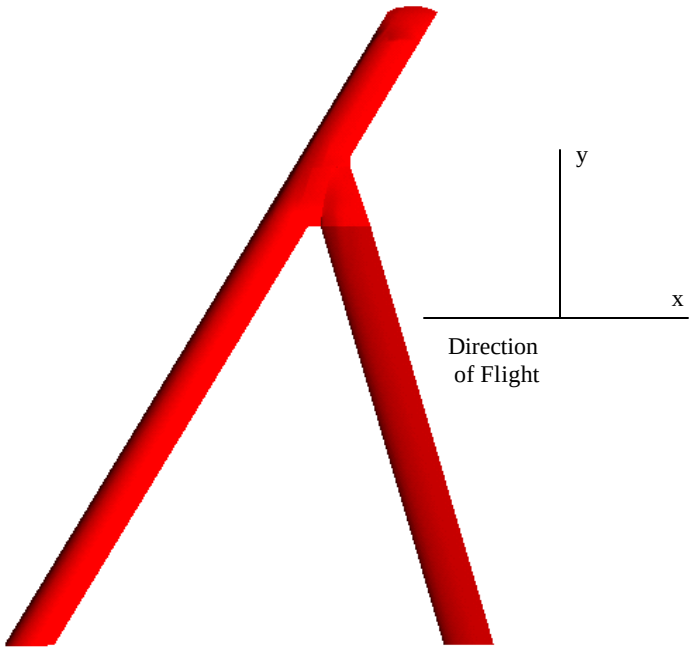

Figure 1-1. Top View of Proposed Joined-Wing Geometry

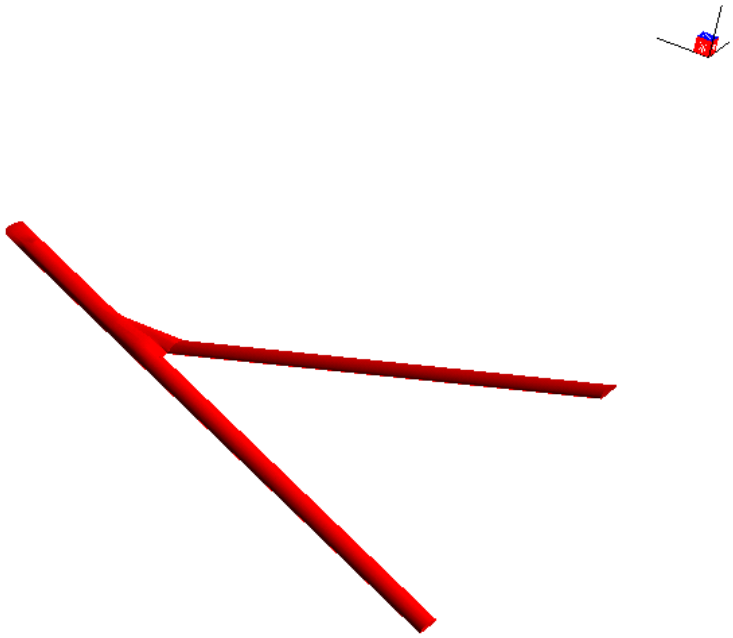

Figure 1-2. Isometric View of Proposed Joined Wing Geometry

The aft-wing acts as a support strut for the cantilevered main wing to relieve bending moments. The aft-wing undergoes axial compression throughout most of the flight regime. This compression may cause the aft-wing to buckle. Studies have proposed that the increased structural weight to prevent aft-wing buckling might negate any performance benefits gleaned from the joined-wing configuration [1].

The proposed sensor-craft wing span is over 180 feet and the chord of the main wing is approximately eight feet. Under normal flight conditions this wing experiences large bending deformations. Linear finite element analysis is an approximation method that is only valid for relatively small displacements. The large deflections of the joined-wing require non-linear finite element analysis method for accurate results.

The large wing deformation also causes a significant change in the aerodynamic pressure distribution. A method to calculate the pressure distribution of a deformed aerodynamic model is used in this research. This method is included in the overall process to achieve an aerodynamically trimmed aircraft.

The current proposed sensor-craft design incorporates radar antennae in the forward and aft-wings. This provides a very large aperture, enabling UHF surveillance. This radar frequency is required for foliage penetration (FOPEN) which allows the radar to image a target beneath a canopy of vegetation [2]. As a proposed weight savings, the antenna elements are built into the composite wing structure. This Conformal Load-bearing Antenna Structure (CLAS) is a composite sandwich of Graphite/Epoxy, Carbon foam core, and an Astroquartz skin covering (Figure 1-3). Antenna elements are attached to the graphite/epoxy layers. The Astroquartz

provides environment protection and an electro-magnetically clear material for the radar to transmit through.

Figure 1-3. Conformal Load-bearing Antenna Structure Cross Section

Adaptive Modeling Language (AML) allows a user to develop a geometric model that contains all necessary information needed to perform multi-disciplinary analysis [3]. The Air Vehicles Technology Integration Environment (AVTIE) is software developed by Dr. Max Blair [4]. AVTIE contains the sensor-craft geometric model. It enables the designer to develop the aerodynamic and structural models. AVTIE also performs aerodynamic trim calculations.

Due to the long-endurance requirement, sensor-craft contains a large amount of fuel mass at the beginning of the mission. The large fuel mass provides inertia relief to the wing structure. The inertia relief helps reduce the amount of deformation caused by the lift generated during flight. However, near the end of the mission, there is very little fuel mass available to counteract lifting forces or accelerations caused by gusts. Therefore, the aircraft structure tends to experience higher stresses at the end of the mission than at the beginning.

Research Objectives

This research achieved a weight optimized sensor-craft structural model that was aerodynamically trimmed and did not buckle or become overstressed during the flight regime. Two models were optimized, one entirely aluminum and one incorporating CLAS and graphite/epoxy material. This research investigated the non-linearity due to large deformations and developed a method to incorporate non-linear analysis into the conceptual design process. In addition, aerodynamic and structural interaction in the model was demonstrated. Also, this study developed an estimate of reliability to quantify the uncertainties in the material properties.

Research Focus

This research focused on developing a cross-disciplinary approach to aircraft design. Aerodynamic analysis and structural optimization were combined to develop a minimal weight aircraft configuration that is aerodynamically trimmed throughout the mission. This research recognizes the need to include non-linear structural analysis due to large deformations.

Methodology Overview

Analysis using high fidelity FEM based modeling techniques and aerodynamic panel methods was executed to optimize a joined-wing configuration for the required sensor-craft mission. Linear fully stressed design using flexible aerodynamic loads at selected mission points was accomplished. The aircraft was aerodynamically trimmed during this design process. Linear analysis continued with various flexible aerodynamic load cases and considered buckling of the aft-wing as a critical design constraint. Optimizing the skin thickness may decrease aircraft weight depending upon stress requirements.

This study also analyzed a non-linear, fully stressed design of the joined-wing configuration for the same mission load cases as the linear analysis. Currently available commercial software packages are not capable of resizing a non-linear FEM. An algorithm is developed in MATLAB code [5] and incorporated into the existing Adaptive Modeling Language (AML) software suite, which provides a geometric interface between MSC.NASTRAN finite element software [6] and PanAir aerodynamic software [7]. Non-linear design allows the aft-wing to undergo large deformation without structural failure. The tailored non-linear response of the aft-wing was incorporated in trim optimization.

The model was first optimized using an aluminum model. This optimized model provided a baseline for comparison to the composite model. It also allowed the researcher to validate the linear and non-linear optimization methods with a simplified model before developing the more complex composite design model.

The optimal material distribution was achieved for the minimum weight for a fixed configuration in both the aluminum and composite models. Stochastic analysis methods were applied to quantify the level of confidence in the buckling loads and stresses based on estimates and assumptions made during the course of this study. Uncertainties in the composite material properties must be considered since the aircraft wing incorporates a Conformal Load-bearing Antenna Structure (CLAS) within the composite wing structure. The material properties for this composite have not been thoroughly studied. These uncertainties are modeled using Gaussian randomness in the Young's modulus throughout the joined-wing. Stochastic sensitivity to the Young's modulus is examined for the aluminum joined-wing structure.

Assumptions and Limitations

For the deterministic analysis of the aluminum model, a factor of safety of 1.5 was applied to the Von Mises allowable stress in the linear optimization method. In the non-linear optimization a factor of 1.5 was applied to the applied loads and no factor of safety is applied to the Von Mises allowable stress. This method allowed the NASTRAN non-linear analysis to provide a complete analysis, and ensureed safe performance up to 150% of the design load.

The leading edge skin and rib elements that are forward of the front spar were not optimized. This is also true for the skin and rib elements aft of the rear spar. These elements are not included in typical wing design models because they are not primary load bearing members. In this model, the un-designed skin elements were set to a minimum gage thickness and the un-designed rib elements were set to a value that is sufficiently thick to transfer any aerodynamic loads into the wing box.

Due to the method AVTIE uses to create the structural model, the wing substructure is highly redundant. The initial design philosophy was to allow the optimization process to determine the best load path by minimizing the redundant structure [4]. Each wing contains eight spars when a typical wing design uses only two or three spars. Also, the wing-joint and outboard wing include spars from both the forward and aft-wings. Thus, the outboard wing contains sixteen spars. The spars in the forward and aft-wings are designed with a minimum gage of 25% of the skin minimum gage thickness. It is assumed that the total optimized spar thickness can be combined into a forward and aft-spar for each wing.

For the composite model, a graphite/epoxy maximum strain allowable of 5000με [8] with a factor of safety of 1.5 was used in the linear optimization method. The wing substructure remained aluminum in this model and was included in the optimization process with the Von Mises allowable stress for aluminum. The non-linear optimization used the maximum strain allowable with a factor of 1.5 applied to the applied loads.

The CLAS material was included as the upper and lower surfaces of the forward and aft-wings. The Astroquartz is a relatively weak material (6.80 Msi) [8] and was not included in the optimization method. Also, the foam core sections are primarily for radar element spacing requirements and were not designed. Each graphite/epoxy layer in the CLAS material is an optimum stacking sequence developed by Northrop Grumman [8]. Thicknesses of the graphite/epoxy plies were determined in the design optimization as necessary to accommodate the applied loads.

Similar to the aluminum model, the skin and rib elements outside the wing box were not optimized. The un-designed skin material is Astroquartz. The leading and trailing edges must be electro-magnetically clear to allow radar transmission. The wing-joint and outboard wing skins are graphite/epoxy. The entire substructure is also graphite/epoxy with the same minimum gage limits as the aluminum model.

The structural NASTRAN model was analyzed using a clamped boundary condition at the forward and aft-wing roots. Ideally, the model would be analyzed using a free-free boundary condition that would include inertia relief due to aircraft structural mass, payload mass, and fuel mass. However, the fuel mass can only be included using non-structural mass elements in

NASTRAN. When conducting optimization using multiple mission points, NASTRAN is unable to use multiple sets of non-structural mass elements to define the different fuel mass at each mission point. AVTIE develops gravity forces due to the mass of each structural element and fuel mass. These forces develop a load case comparable to the free-free boundary condition. The clamped boundary condition and the free-free conditions of a single load case were compared to validate the use of the simplified boundary conditions.

A concurrent study is underway to incorporate aerodynamic results from MSC.Flight Loads software into the AVTIE environment. Flight Loads can trim the configuration and export the model directly to NASTRAN. The Flight Loads and PanAir panel methods will be compared elsewhere with a Euler/Navier-Stokes CFD code for validation [9].

Implications

This multi-disciplinary approach to aircraft design provides a method that encompasses all aspects of the conceptual design process. This allows a designer to observe and incorporate the interactions of structural and aerodynamic effects. AVTIE also allows the researcher to study the magnitude of non-linearity due to large deformations. This research demonstrated the ability to integrate multiple iterative processes into a single optimization method. Potentially, AVTIE is capable of developing an optimized conceptual design for any aircraft configuration.

Preview of Results

Initial linear optimization demonstrated aerodynamic and structural convergence to an optimized design (Table 4-1). The mass redistributed to a similar optimized material distribution as described by Wolkovich [10] (Figures 4-4, 4-5).

Because the aft-wing is closely aligned with the joined-wing plane, the material distribution is very close to the optimal structure proposed by Wolkovich. Non-linear optimization exhibited similar material distribution. The composite model also optimized to a similar mass distribution.

Non-linear analysis exhibited larger deformations and higher stresses than linear analysis. The non-linear analysis also demonstrated that the model behaved in a non-linear fashion well below the first buckling eigenvalue.

Preview of Conclusions

The model is highly coupled between aerodynamic loads, structural deformation, and aerodynamic trim. This sensor-craft configuration behaves as a non-linear structure below the first buckling eigenvalue.

II. Literature Review

Introduction

This chapter summarizes the relevant joined-wing structural and aerodynamic research already accomplished. First, it reviews the advantages gained with this design and highlights some of the structural nuances of the joined-wing. Next, the chapter highlights the issues encountered in designing such an aircraft.

This chapter discusses past research in the areas of non-linear structural analysis and structural optimization. It also makes note of differences between the past research and this current thesis. In addition, this chapter reviews a proposed method of aerodynamic and structural optimization. The chapter continues with an overview of a preliminary stochastic analysis of a joined-wing. The chapter concludes by describing the sensor-craft configuration that this thesis research builds upon.

Past Joined-Wing Design Work

Julian Wolkovich proposed a joined-wing design in 1976 [11]. In a later study, he claimed the design provided potential weight savings and aerodynamic benefits [10]. In addition to a lighter aircraft weight, Wolkovich claimed a properly designed joined-wing would have reduced induced drag, high maximum lift coefficient (C_{Lmax}), lower parasitic drag, and improved stability and control characteristics [10].

Wolkovich observed that the lifting forces of the forward and aft wings can be resolved into forces normal to and parallel to the structure of the joined-wing (Fig. 2-1). The force normal to the plane containing the forward and aft-wing structure causes a bending moment about the z-axis.

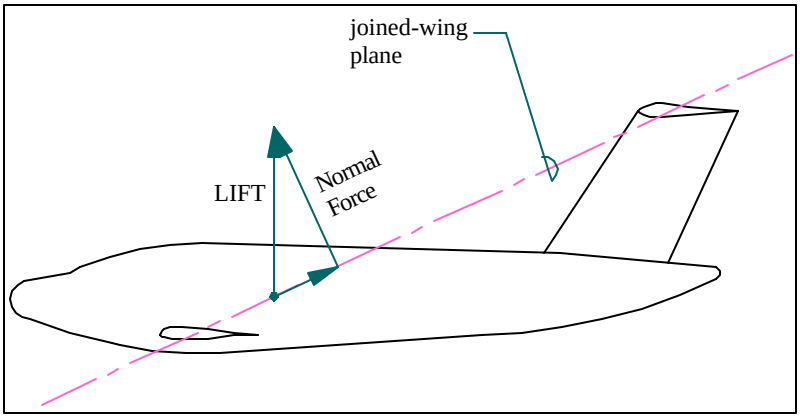

Figure 2-1. Normal Force in Joined-Wing Plane [10]

With a vertical force applied to the joined-wing, the forward wing tip displaces in the positive z-direction and the negative x-direction. The bending axis becomes aligned perpendicularly to the plane of the joined-wing structure, that is, the plane containing the span-wise axes of the forward and aft-wings. In an optimum cantilever design, structural material is located away from the neutral axis. This increases the moment of inertia and decreases bending stress. Typically, this requirement creates a wing box structure of constant thickness at each cross section [10]. The joined-wing also requires structural material to be placed away from the neutral surface to relieve stress. However, placing material at the maximum offset distance possible creates a wing box structure that is thicker at the upper leading edge and lower trailing edge (Fig. 2-2).

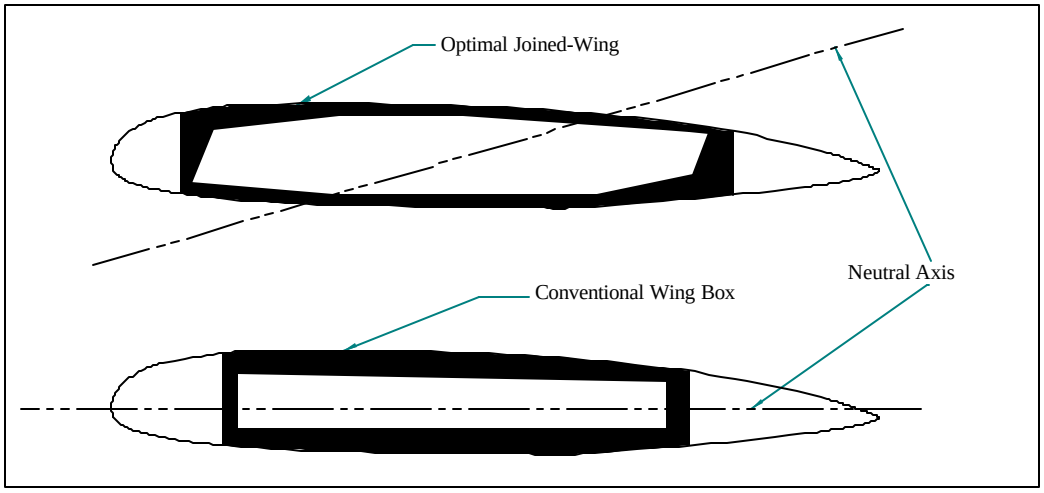

Figure 2-2. Optimal Joined-Wing Structure vs. Cantilever Wing Structure

An optimized joined-wing structure resists bending with a thinner airfoil than a cantilever wing box structure. The thinner airfoil also creates less induced drag. Wolkovich cautions that a thin aft-wing is more likely to experience column buckling than a thicker wing.

Wolkovich compared the available fuel volume in a joined-wing to that of conventional, cantilevered wings. Because of the additional volume available in the aft-wing, the joined-wing potentially contained 150% of the fuel available in a conventional design [10]. This could allow the joined-wing greater range and endurance.

Structural optimizations of the sensor-craft model display the increased material thickness in the upper leading edge and the lower trailing edge. The model also exhibits the negative-x deflection noted by Wolkovich. The success of sensor-craft depends on the ability to remain aloft for over forty-eight hours. This drives the fuel mass requirement much higher than a conventional aircraft.

Samuels continued Wolkovich's earlier studies to validate the potential weight savings of a joined-wing over a conventional aircraft [12]. She compared two joined-wing configurations to a Boeing 727 design. The joined-wing configurations were identical except the minimum skin thickness. All models used aluminum structural material. The joined-wing cases were structurally optimized for a 2.5-G load case, with a 1.5 factor of safety, using allowable Von Mises stress as the design criterion [12]. Optimized, the joined-wing models exhibited the thickening of the upper leading edge and lower trailing edge. The optimization study indicated that both joined-wing cases were lighter than the conventional aircraft design [12]. Although the joined-wing models were lighter, Samuels cautions that the designs were selected as a comparison to the Boeing 727 and may not be the best joined-wing design. Samuels did not include buckling as a design constraint, nor did her research consider non-linearities caused by large deformations in the finite element model.

This sensor-craft study investigates one configuration for a specific, long endurance mission. In this current study, the minimum gage thickness is set at 0.040 in. for the aluminum cases based on standard aircraft aluminum manufacturing practices [13]. Samuels, used 0.125 in. and 0.070 in. as minimum gage thickness. The larger minimum gages may have prevented a fully optimized design.

In 1984, the NASA Ames Research Center initiated research into the possibility of building a joined-wing airplane [14]. NASA designed the aircraft to be a manned, proof-of-concept demonstrator. The requirement of human survivability dictated the requirement to create good handling qualities. Smith et al. observed the joined-wing configuration reduces the bending

moment of the forward-wing, and calculated the span efficiency to be higher than 1.0 [14]. The span efficiency is the ratio of the induced drag created by an elliptical lift distribution to the induced drag created by the actual lift distribution [14]. This increased efficiency validated the earlier claim of reduced drag [10]. The researchers discovered that even with extensive aerodynamic design, the one-sixth-scale wind tunnel model exhibited an unstable stall characteristic [14]. The scale model also had reduced lateral stability above the stall angle-of-attack. The stall characteristic was improved with vortilions installed on the wind tunnel model, but a full-scale flight test vehicle was never built. It should also be noted that there was no structural optimization design performed. Where buckling was predicted, the tail structure was strengthened with additional material [14].

Extending the research for the NASA Ames feasibility study, Lin, Jhou, and Stearman examined the joint configuration using the NASA wind tunnel model [15]. The researchers studied eight different joint models on a joined-wing wind tunnel model similar to the NASA aircraft. They employed linear Finite Element Modeling (FEM) analysis and experimental analysis on the one-sixth-scale wind tunnel model. This study also used a simplified FEM model incorporating CBEAM and QUAD4 elements. The MSC.NASTRAN analysis indicated a lower root bending moment than the experimental results. The authors attributed this difference to the absence of friction in the finite element model [15]. They discovered that the best joint designs are a rigid joint or a pinned joint with the z-axis free to rotate [15]. The sensor-craft configuration in this thesis research uses a rigid joint configuration.

Work of Gallman and Kroo

Kroo et al. developed a method to optimize a joined-wing configuration for aerodynamic and structural characteristics using several design variables [16]. Their method used a vortex-lattice aerodynamics code to trim the joined-wing aircraft for a minimum drag condition. The method then used a finite element code to optimize the design for minimum weight [16]. They also included an asymmetric wing box structure similar to the design proposed by Wolkovich. In all configurations studied, the aft-wing carried a negative lift load to achieve a trimmed flight condition. This negative lift cancelled the expected reduction in induced drag. "…Induced drag reductions are only possible when the aft surface carries a significant upload" [16]. By varying the location of the wing-joint, the authors realized a large reduction in weight when the wing-joint was placed at 70% of the forward-wing span [16]. Only linear FEM analysis was performed on the joined-wing design. The authors state that the linear analysis was sufficient provided the structure did not undergo large deformations or buckling [16]. They observed that in all cases the aft-wing carried a large compressive load and the forward-wing had a lower wing-root bending moment than a conventional wing [16]. The researchers stressed that future studies should include buckling analysis of the aft-wing.

This sensor-craft research includes non-linear fully stressed design to incorporate large deflection analysis. While Gallman and Kroo state that they performed an aerodynamic analysis, their paper does not mention achieving an aerodynamic trim condition for the structurally optimized model. This thesis incorporates the aerodynamic analysis as part of the convergence processes. This develops a minimum weight design that is also aerodynamically trimmed.

Later, Gallman and Kroo refined the aerodynamic analysis and compared their models to a McDonnell Douglas DC-9 conventional transport [17]. The researchers determined that the critical load conditions occurred during gust conditions that describe the flight envelope. The joined-wing models used a 10% average thickness airfoil. The Sensorcraft model studied here has a 15% average thickness airfoil. Using direct operating cost as a design objective, they determined that the joined-wing model was more expensive to operate when buckling constraints were included in the design analysis. Gallman and Kroo did not use non-linear structural design for potentially large deflections in this study. They also incorporated a fuel tank in the aft wing to trim the center of gravity [17]. This sensor-craft research utilizes the fuselage payload mass to adjust the center of gravity and maintain a aerodynamically stable, mass-balanced condition throughout the mission profile.

Gallman and Kroo also examined a joined-wing configuration to meet the mission requirements of a Boeing 727 transport aircraft [1]. They used a simplified aluminum wing box structure in the FEM analysis. The authors determined that the gust during zero fuel condition was the most critical load case [1]. However, they do not mention the use of a gust alleviation factor to reduce the effective gust load. This simplified model was optimized for a minimum weight using gradient-based design. Next, they optimized the model again using fully stressed design and included the secondary bending moments to capture the non-linear effect [1]. When Gallman and Kroo included buckling as a design constraint in their gradient-based optimization analysis, the weight increased by 13%. This led to a higher direct operating cost when compared to a Boeing 727. The fully stressed design with secondary bending moments did not include a margin of

safety [1]. They determined that the fully stressed design was comparable in weight to the gradient-based design but still higher in weight and direct operating cost than the conventional aircraft. However, they conceded, "a different set of mission specifications and design assumptions may produce joined wings that perform significantly better"[1].

Current sensor-craft research uses fully stressed design instead of gradient-based design due to the large number of design variables used. NASTRAN non-linear finite element analysis data is combined with MATLAB fully stressed design algorithm to create a non-linear fully stressed design process. Importantly, this research structurally optimizes a joined-wing model while maintaining aerodynamic trim. Gallman and Kroo performed aerodynamic analysis, but did not integrate aerodynamic trim analysis within the optimization process.

Integrated Structural and Aerodynamic Design

Recently, Livne surveyed past joined-wing research to provide a direction for future studies [18]. He described how the joined-wing configuration creates complex interactions between aerodynamic loads and structures. He also noted that slender beam models, such as the joined-wing configuration, should be modeled as non-linear structures to capture moderate to large deformations. Livne advocated the use of a multi-disciplinary design approach to design aerodynamics and structures simultaneously [18].

Blair and Canfield proposed an integrated design method for joined-wing configurations [4]. They chose the model configuration to meet the sensor-craft mission requirements. The concept utilized the entire aft-wing as a control surface for pitch trim. The aft-wing was twisted

through the use of an actuator in the vertical tail. This created torsion in the aft wing and a twist angle that decreases from the root to the wing joint. As in previous studies, Blair and Canfield used a rigid wing joint for the model. Their concept started with an initial estimate of fuel required to complete the desired mission and a constant lift-to-drag ratio. Next, they trimmed the aircraft for straight and level flight conditions throughout the mission. The authors cautioned that a large angle-of-attack or aft-wing twist angle created excessive drag and should be avoided. They also indicated that a negative lifting force on the aft-wing increased drag [4]. The aerodynamic loads and the trimmed configuration were used to perform a linear fully stressed design optimization in ASTROS finite element software. The authors checked for buckling using NASTRAN. This optimization resized the wing skin, rib and spar thickness to meet the allowable material stresses. The deflection of the wing caused a different lift distribution over the wings, which required a new trim configuration. The deformed model was re-trimmed and the new aerodynamic loads were applied to the structural model [4].

Blair developed a geometric model and user interface, known as Air Vehicle Technology Integration Environment (AVTIE) [4] using the Adaptive Modeling Language (AML)[3]. The AML model can be analyzed for structural or aerodynamic characteristics through external software. Aluminum was used in their study although the sensor-craft will most likely use composite structure [4]. Similar to Gallman and Kroo [1], Blair and Canfield also recognized that a critical load occurs at the minimum fuel condition [4]. However, their load case assumed a steady 2.5G maneuver instead of a gust condition. When the researchers analyzed buckling of the optimized model, they discovered that the forward-wing buckled beyond the applied 2.5G load,

but before the 1.5 factor of safety. The aft-wing buckled in a non-trimmed condition. They concluded that non-linear structural analysis is important to accurately capture the large deformations and buckling behavior that occur in this large joined-wing configuration. Also, the authors discovered that for some critical buckling modes, the outboard wing tip becomes aerodynamically unloaded. They noted this buckling as a possible means for creating a fail-safe design [4].

This current research starts with the same model configuration as Blair and Canfield [4]. However, multiple mission conditions are optimized and aerodynamically trimmed simultaneously. Gust loads develop higher load factors than steady load cases and are included in the optimization. Linear fully stressed design and buckling analysis was performed using NASTRAN instead of ASTROS. A MATLAB non-linear fully stressed design algorithm was used to capture large deformations. This research heavily utilizes AVTIE for aerodynamic trim and model generation.

Stochastic Analysis

Petit, Canfield and Ghanem conducted a stochastic analysis on a joined-wing model developed by Blair and Canfield [19]. The buckling of the joined-wing was analyzed using NASTRAN. Buckling analysis requires the solution to a linear eigenvalue problem. The random Young's modulus is a component of the stiffness matrix used for the buckling solution. The authors modeled Young's modulus as a Gaussian random variable at the wing-roots and the wing-joint. These locations were expected to have the most critical influence in the buckling response of the joined-wing [19]. They conducted a Monte-Carlo simulation using 200

realizations of the random Young's modulus at each location. NASTRAN generated a buckling eigenvalue solution for each of the realizations, which estimated the random distribution of response. The authors conducted a sensitivity study to examine the influence of each location on the overall buckling solution. The initial eigenvalue solutions had a margin of safety greater than 34%[19]. The Young's modulus was significantly reduced at each location to increase the sensitivity. However, the model exhibited very little sensitivity to reductions in the stiffness [19]. The sensitivity study confirmed the author's premise that the outboard wing joint would have the least effect on the buckling solution [19]. The authors concluded that the random Young's modulus should be applied throughout the model. Also, they suggested that the aerodynamic loads be modeled as random variables [19].

Choi, et al expanded on the Monte-Carlo simulation method by using a Latin hypercube sampling of the polynomial chaos expansion [27]. This was determined to be a computationally efficient procedure to quickly develop statistical data for a large finite element model with random material properties. This current sensor-craft research employs this method to provide initial statistical data.

Basis for Current Research

This research will continue the work of Blair and Canfield [4]. To utilize the multi-disciplinary design method developed by the authors, I incorporate non-linear finite element analysis into this design method as well as the rigid joint configuration suggested by Smith et al. [15]. Also, the FEM model used will be a highly detailed wing design unlike the simplified models used by Gallman and Kroo [1], Samuels [12], and Lin et al. [15]. These features create a model

that provides a more accurate representation of the aircraft as presently conceived. In addition, it includes composite materials in the joined-wing structural analysis and optimization.

III. Methodology

AVTIE Model and Environment

The Adaptive Modeling Language, developed by TechnoSoft Inc., allows the researcher to develop a geometric model through mathematical relationships [3]. Blair and Canfield have developed the Air Vehicles Technology Integration Environment (AVTIE) [4], which provides a user interface to the AML software capabilities. The AVTIE code builds a geometric surface

model from configuration data defined in three text files. Appendix A contains text of the baseline configuration files and a display of the AVTIE user interface. Figure 3-1 displays the parameters of the geometric surface developed from the configuration files. AVTIE converts the geometric model into data files for analysis with external software such as PanAir and NASTRAN. AVTIE also interprets the output data from these programs and updates the geometric model as required. Table 3-1 lists the relevant geometric properties for the baseline configuration. This study did not alter the aerodynamic planform properties of the model during optimization.

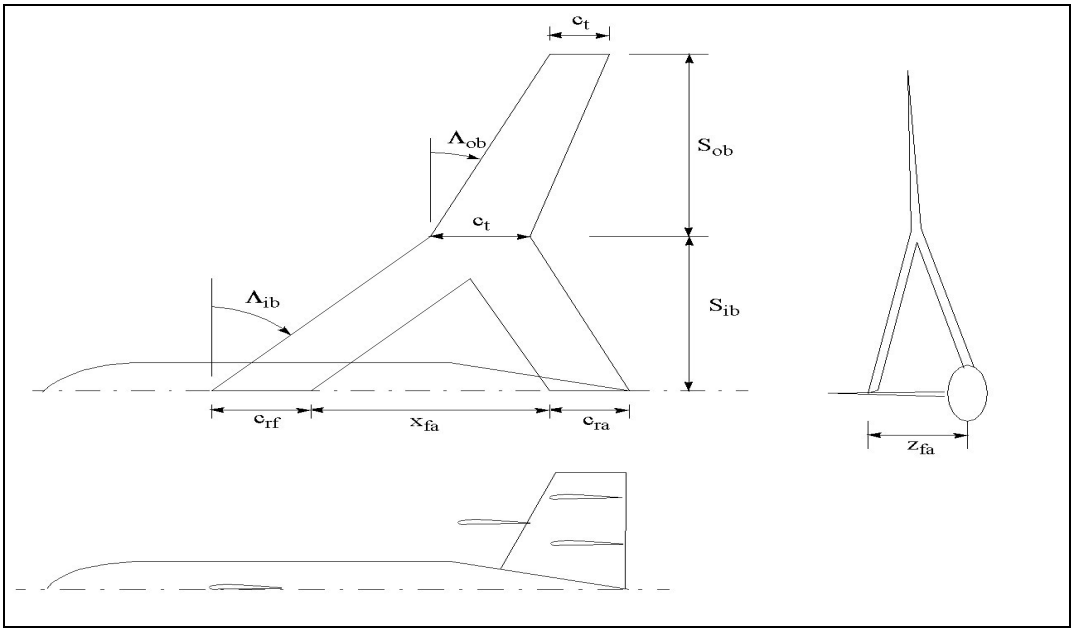

Figure 3-1. Planform Configuration [4]

Inboard Span	S_{ib}	26.00 m
Outboard Span	S_{ob}	6.25 m
Forward Root Chord	c_{rf}	2.50 m
Aft Root Chord	c_{ra}	2.50 m
Mid Chord	c_m	2.50 m

Tip Chord	c_t	2.50 m
Forward-aft x-offset	x_{fa}	22.00 m
Forward-aft z-offset	z_{fa}	7.00 m
Inboard Sweep	Λ_{ib}	30 deg
Outboard Sweep	Λ_{ob}	30 deg
Airfoil		FX-60-126-1
Calculated Planform Area		145.0 m^2
Calculated Wing Volume		52.2 m^3

Table 3-1. Baseline Configuration Parameters [4]

The AVTIE software contains information about the mission profile (altitude, airspeed, fuel consumption rate, etc.). The mission profile reflects the current Global Hawk surveillance mission requirements. Since this study did not optimize or adjust the mission requirements, these constraints were embedded in the software code and were not changed. AVTIE separates the mission into three categories; ingress, loiter, and egress. Mission legs are sequentially numbered starting at zero. Table 3-2 displays the mission properties used in this study.

	Ingress (0)	Loiter (1)	Egress (2)
Range	3000 nm 5,550 km	NA	3000 nm 5,550 km
Duration	NA	24 hr 8.64E4 sec	NA
Velocity	0.6 Mach @50K ft 177 m/s	0.4 Mach to 65K ft 118 m/s	0.6 Mach @50K ft 177 m/s
C (SFC)	2.02E-4 (1/sec)	1.34E-04 (1/sec)	2.02E-4 (1/sec)
Dynamic pressure	2939 Pa	638 Pa	2939 Pa

Table 3-2. Baseline Aerodynamic Parameters [4]

AVTIE further reduces the mission categories into a fraction of completion for each mission leg. For example, when half of the egress portion is completed, AVTIE defines this mission point as 2.50. AVTIE uses the performance information to provide the weight of the remaining fuel at any point in the mission. Although AVTIE provides for empirical drag calculation, currently the Lift-to-Drag ratio (L/D) remains fixed throughout the mission. The constant L/D enters the calculation of fuel required through the Breguet range equation (Equation 3-1) [20]. In this research only the change in structural weight altered the fuel required.

$$R = \left(\frac{V}{C}\right)\left(\frac{L}{D}\right)\ln\left(\frac{W_{i-1}}{W_i}\right) \tag{3-1}$$

The sensor package (payload) has an estimated mass of 2200 kg and is placed within the fuselage. It is assumed that the payload is a 'black-box' that can be placed in the fuselage based on the mass balancing requirement.

AML stores material properties in a separate data file for easy editing (Appendix A). Initial material properties were for 2024-T3 aluminum. AVTIE can not incorporate composite material data due to the need to create individual ply layers within each structural element. Also, the CLAS material data was required to account for the radar material embedded in the inboard wing skin. Once the composite structural element thicknesses were optimized via fully stressed design; an element thickness was returned to AVTIE that corresponded to the optimized element mass but using aluminum material density. A cyanate-ester composite (Astroquartz) material covers the antenna material [8] and is used in the leading and trailing edge skin elements. This material allows the embedded antenna to transmit with minimal interference. AVTIE initially

defines a uniform element thickness for all structural components. The AVTIE-generated aluminum structural model was converted into a multi-material composite and aluminum model.

Materials

The linear and non-linear structural optimization and aerodynamic trim process was carried out for both the aluminum and composite models. The aluminum model used 2024-T3 aircraft aluminum with a minimum skin thickness of 0.04 in (1.016E-3 m). Table 3-3 lists the material properties [26].

	KSI	MPa
σ_{ty}	47.0	324.05
σ_{cy}	39.0	268.90
σ_{shear}	39.0	268.90
E	10.5E+3	72395.0
G	4.0E+3	27580.0

Table 3-3. 2024-T3 Aluminum Material Properties

An allowable Von Mises stress (σ_e) was developed using [23]:

$$\frac{1}{\sqrt{2}}\sqrt{s_x^2 + s_y^2 + 6\cdot\left(t_{xy}^2\right)} = s_e \qquad (3\text{-}2)$$

Compressive yield stress (σ_{cy}) was used as the allowable stress in the x and y directions. Also, the shear stress (σ_{shear}) was reduced by a factor of 0.577. The sensor-craft was modeled using plate elements that take transverse shear. However, the wing box design allowed the skin elements to take the majority of bending stress and the spar elements to take in-plane shear. The equation for Von Mises stress reduced to:

$$\frac{1}{\sqrt{2}}\sqrt{\left(2s_c^2\right)+6\cdot\left(\frac{s_s}{\sqrt{3}}\right)^2}=s_e \qquad (3\text{-}3)$$

The Von Mises stress was calculated with a 1.5 factor of safety as 253×10^6 Pa (36.7 ksi) and was used as the allowable stress constraint in the linear fully stressed design. In the non-linear design, the allowable stress was the Von Mises stress without the 1.5 factor of safety, 379×10^6 Pa (54.9 ksi). To maintain a factor of safety, the loads used in non-linear analysis were increased to 150% of the calculated loads. This optimized the wing structure to withstand a load 150% greater than the calculated flight load.

The composite model incorporated CLAS material on the upper and lower surfaces of the forward and aft-wings inboard of the wing-joint. The CLAS material is a sandwich structure of graphite/epoxy, Astroquartz and carbon foam. The antenna elements are embedded attached to the graphite/epoxy layers. The carbon foam acts as spacing for the antenna elements. Figure 1-3 depicts the CLAS material configuration.

The composite configuration used graphite/epoxy ribs and spars that were structurally optimized in the fully stressed design. This composite material was designed with the same material properties as the composite skin.

IM7/977-3 graphite/epoxy was used in the CLAS structure and was used in the non-antenna wing skin areas as well [8]. Table 3-4 lists the typical material properties used in this analysis.

E_x	22.13E+3 ksi	1.53E+11 Pa
E_y	2.15E+3 ksi	1.48E+11 Pa
ν_{xy}	0.3	0.3
G_{xy}	0.6E+3 ksi	4.14E+9 Pa
t_{ply}	0.0056 in	1.42E-4 m

Table 3-4. IM7/977-3 Material Properties [8]

The IM7/977-3 composite has a maximum allowable strain of 5000με (0.5%). Using a factor of safety of 1.5, the allowable strain in linear design was set to 3333με (0.33%). As in the aluminum model, the non-linear design used the maximum allowable strain (5000με) and increased the loads by 150%. The design optimization used a lay-up of [+45/-45/0/90] for each section of the CLAS material and the same lay-up for the designed, non-CLAS wing skin elements. To approximate adding additional layers, a design variable was assigned to each ply. As the structural, fully stressed design optimization required, each ply was thickened or thinned. The minimum allowed value was a ply thickness equivalent to the designed number of plies in the lay-up created by Northrop Grumman for each orientation in the lay-up [8]. In the CLAS material, each ply orientation was assigned a single design variable for both graphite/epoxy layers.

For example, if the 0° ply in the lower graphite/epoxy layer required an increase in thickness, the 0° ply in the upper layer was increased by the same amount.

In the outboard wing and wing-joint area, the skin elements were a single graphite/epoxy layer with a minimum design of a single ply thickness in each orientation. The un-designed material outside the wing box structure was changed from aluminum to Astroquartz II/RS12-B to allow clear radar transmission through the wing. The properties for Astroquartz are listed below in Table 3-5.

E_x	6.80E+3 ksi	4.68E+10 Pa
E_y	1.34E+3 ksi	9.23E+9 Pa
ν_{xy}	0.36	0.36
G_{xy}	0.72E+3 ksi	4.96E+9 Pa
t_{ply}	0.0055 in	1.40E-4 m

Table 3-5. Astroquartz II/RS12-B Material Properties [8]

The Astroquartz material was not optimized in this model. The Astroquartz has approximately one-third the strength of the graphite-epoxy and does not contribute significantly to the strength of the wing structure. Eighteen plies of Astroquartz were used in the CLAS material and in the un-designed wing areas.

Justification for Gust Load

Gust conditions created higher aerodynamic load factors than stable maneuver conditions for this design. In straight and level 1.0G flight, the lift load equals the aircraft weight. If the aircraft enters a gust condition, the velocity of the gust rapidly increases the angle of attack.

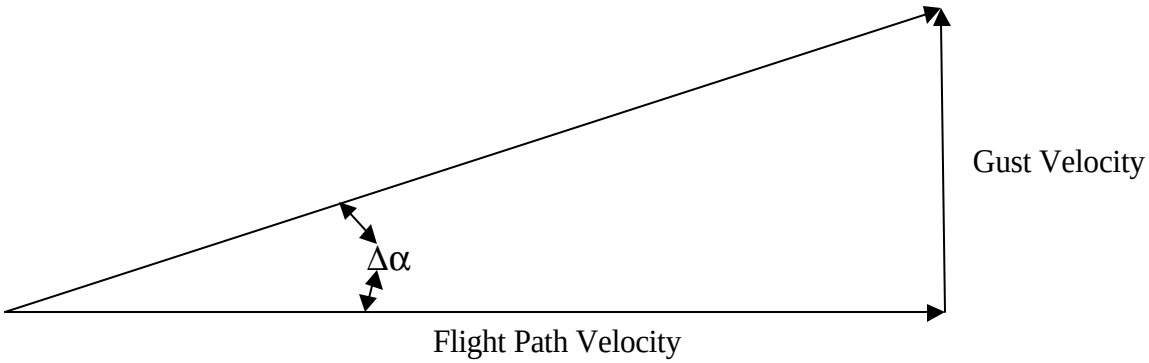

Figure 3-2. Change in Angle of Attack Due to Gust Velocity

This change in angle of attack increases the lift by ΔL and causes acceleration greater than the 1.0G weight [20]. However, the change in lift due to the gust is unaffected by the weight of the aircraft.

$$\Delta a = \frac{U_g}{V} \tag{3-4}$$

$$\Delta L = a \cdot \Delta a \cdot \frac{1}{2} \cdot r \cdot V^2 \cdot S \tag{3-5}$$

$$\Delta n = \frac{\Delta L}{W} \tag{3-6}$$

For a given velocity and angle of attack, the load factor due to a gust condition increases as the weight decreases [22]. A lighter aircraft will have a higher acceleration than a heavier aircraft at the same gust and flight conditions. Therefore, a gust at the end of the mission with minimum fuel mass will cause the highest load factor increase.

The gust load calculated above assumes an instantaneous gust applied to the entire aircraft. Typically, an aircraft will fly into a gust condition. For a large aircraft, gradually flying into the gust will reduce the load factor encountered. This is known as the gust alleviation factor K [22] defined as:

$$K = \frac{0.88 \cdot m_g}{5.3 + m_g} \tag{3-7}$$

$$m_g = \frac{2 \cdot W}{S \cdot r \cdot a \cdot c \cdot g} \tag{3-8}$$

where μ_g is the airplane mass ratio. The gust alleviation factor is applied to the gust velocity, KU. The gust alleviation factor is dependent on the wing loading (W/S) of the aircraft. A higher wing loading increases the gust load factor.

For a large aircraft, the gust conditions are taken as 50 ft/s at cruise velocity, V_C and 66 ft/s at design speed for maximum gust intensity, V_B [12]. The design maneuver speed, V_B is at least 43 knots less than cruise speed [12]. The gust velocities occur in the positive and negative directions. These speeds are used up to 20,000 ft. Above 20,000 ft, the gust speeds decrease linearly [22]. Gallman and Kroo used the same gust velocities in their joined-wing research [1]. They also found that the buckling critical loads were gust loads applied to an aircraft without fuel mass.

Linear fully stressed design using a 2.5G maneuver load at several mission points created a minimum weight design that is not buckling critical. Buckling depends on compressive stresses. The applied aerodynamic and inertia loads indirectly create compression in the aft-wing through the bending moments generated. Therefore, the applied loads must be greatly increased in order to create a significant increase in the compressive stress in the aft-wing. Gust loads can create a large aerodynamic load that is not entirely relieved by the inertia forces. These loads create sufficient compressive stress in the aft-wing to buckle the structure.

Developing Gust Loads in AVTIE

AVTIE sets the altitude as constant for each mission leg. At the end of the mission, the altitude is still set to 50,000ft. The dynamic pressure, which is used in PanAir to develop the aerodynamic loads, was manually changed to develop aerodynamic loads at 20,000ft for gust conditions. The sensor-craft model was then aerodynamically trimmed for a straight-and-level, 1G flight. This flight condition was transferred to NASTRAN for linear static analysis with the current element thickness data. No optimization was performed on this model. The linear static

deformations were returned to AVTIE and the model was trimmed using the deformations and the 1G flight condition. Once the model was trimmed, the gust angle of attack $\Delta\alpha$ (Equation 3-4) was manually calculated and added to the trimmed angle of attack. New aerodynamic loads were calculated through PanAir. The new loads were applied to the structural model for use in the multiple load case, fully stressed design optimization.

Non-Aerodynamic Loads

Another critical load case occurred during taxi at the beginning of the mission for this design. The aircraft is loaded with full fuel mass and the wing surfaces are generating no appreciable lift. If the aircraft taxis over a crater or pothole, the wing will experience a large positive acceleration due to the fuel mass. This load causes the aft-wing to undergo large tension forces that are not normally experienced during flight. For this research, the taxi crater impact load was assumed to be 1.75G for rigid landing gear. It was assumed that the landing gear design and taxi speed could be tailored to meet this load requirement.

The landing impact load was also analyzed. Since sensor-craft is a remotely piloted vehicle, the controller may not have the ability to land the aircraft with exact precision and minimal impact loading. Thus, this research estimates a landing load factor of 3.0G based on conceptual design practices [22]. The landing load case was not critical, because the weight of the aircraft is minimal at the end of the mission.

PanAir Aerodynamic Analysis

PanAir analyzes an aerodynamic model consisting of panel elements. Figure 3-3 depicts the current baseline PanAir panel configuration that AVTIE generates.

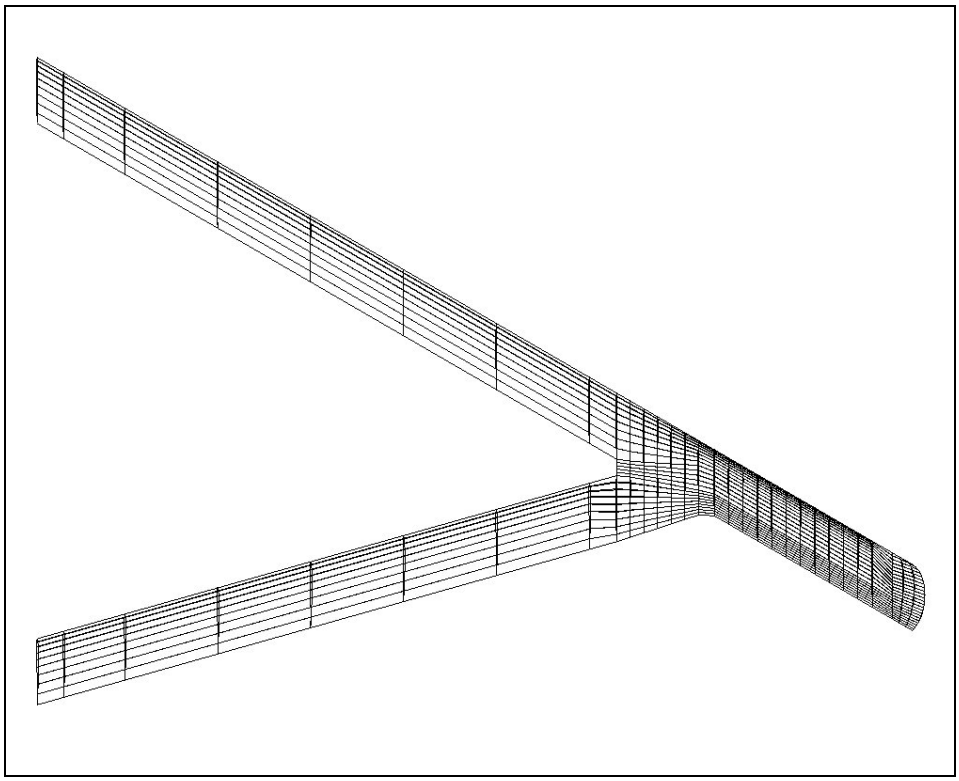

Figure 3-3. PanAir Baseline Geometry with 30 Degrees Sweep (Plan View) [4]

AVTIE provides PanAir with dynamic pressure information based on the mission point to be analyzed. Also, AVTIE transfers angle of attack and aft-wing twist information specified by the designer to PanAir. PanAir calculates interpolated pressures at the panel corners. The interpolated pressures are integrated by AVTIE and distributed over the structural model's forward and aft-wings. AVTIE provides aerodynamic center and center of pressure information as well as total lift and induced drag forces. The PanAir model used in this research is the same as developed by Blair and Canfield [4].

A concurrent study is underway to incorporate aerodynamic results from MSC.Flight Loads software into the AVTIE environment. Flight Loads can trim the configuration and export

the model directly to NASTRAN. The Flight Loads and PanAir panel methods will be compared with a Euler/Navier-Stokes CFD code for validation [21].

NASTRAN Linear Finite Element Analysis

Based on the integrated PanAir pressure distribution, AVTIE transfers the aerodynamic loads to the structural model. AVTIE then creates the NASTRAN input file based on the structural model and load conditions. AVTIE creates a linear static analysis input file with uniform skin thickness throughout the model, even if AVTIE contains element thickness data from a previous optimization or updated model. The thickness of an element is defined in NASTRAN through a property entry known as a PSHELL card. Thus, to design the thickness of each individual element, each element must refer to an individual PSHELL card. NASTRAN computes element displacements and stresses due to the load conditions imposed on the model. NASTRAN uses user-defined design variables to accomplish a linear fully stressed resizing of each element within the wing-box structure. Fully stressed design increases element thickness to meet the allowable stress requirements and decreases element thickness when the element stress is less than the allowable stress. The fully stressed design equation for individual element resizing is:

$$t_{new,i} = \left(\frac{s_i}{s_{allowable,i}} \right)^a t_{old,i} \tag{3-9}$$

This resizing achieves a structure that meets the allowable stress in each element and is a minimum weight design. Equation 3-9 is also used in the fully stressed design for the composite

model. However, the composite model is resized using maximum strain allowable in place of maximum stress allowable (Equation 3-10). The resizing method remains the same.

$$t_{new,i} = \left(\frac{e_i}{e_{allowable,i}} \right)^a t_{old,i} \qquad (3\text{-}10)$$

AVTIE does not create the information NASTRAN requires to perform fully stressed design. NASTRAN requires an individual design variable for each element thickness to be resized. The design variables are defined in DESVAR cards. The DESVAR cards specify a starting thickness as well as maximum and minimum thickness for each element. The design variables are then related to an element thickness through the DVPREL or design variable-property relationship cards. These cards specify the design variable that relates to a specific element thickness.

To resize the elements according to equation 3-9 or 3-10, NASTRAN must develop the Von Mises stress or the strain in each element. The design response (DRESP1) cards specify which type of stress or strain information to create for each element. The design constraint cards (DCONST) specify the upper and lower bounds of the response. The fully stressed design algorithm uses this constraint information as the allowable stress or maximum strain limits. Figure 3-4 displays the relationship of all the NASTRAN design data, property entries, and elements.

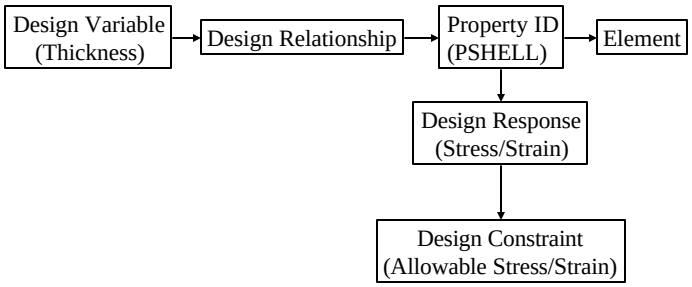

Figure 3-4. NASTRAN Fully Stressed Design Input Data

AVTIE does not produce any of these fully stressed design data entries. A MATLAB code was created to develop the fully stressed design input file from the uniform thickness, linear static analysis files that AVTIE creates and thickness data from a previous optimization, if available. If previous optimization data is unavailable, the MATLAB code used the uniform thickness from AVTIE as the starting point of the fully stressed design.

NASTRAN is able to perform fully stressed design for multiple load cases simultaneously. NASTRAN resizes each element based on the element's highest stress over all load cases. The MATALB code created the input file using multiple mission load cases including taxi crater impact, landing impact and gust load conditions. AVTIE generated the individual load cases for the gust and maneuver conditions. Once NASTRAN completed the analysis, MATLAB created element thickness and displacement files formatted for AVTIE use. This data was used to update the baseline model weight and deflections, which, in turn, are needed to recalculate the flexible aerodynamic loads and trim.

NASTRAN performs non-linear analysis for a single load case only. NASTRAN is also unable to perform non-linear fully stressed design. Therefore, additional MATLAB code was created to execute NASTRAN non-linear analysis for each load case and perform the fully stressed design algorithm within MATLAB.

NASTRAN Non-Linear Structural Analysis

For a finite element model involving small displacements, the linear strain/displacement relationship is valid.

$$e_{ij} = \frac{1}{2}\left(\frac{\partial u_i}{\partial x_j} + \frac{\partial u_j}{\partial x_i} \right) \tag{3-11}$$

Equation 3-11 is a Taylor series approximation ignoring the higher order terms. For large deformations, this approximation becomes invalid.

In finite element analysis, the element strain/displacement relationship is represented as:

$$\{e\} = [B]\{u\} \tag{3-12}$$

where [B] is the derivative of the shape function matrix [N], at the current deformed model geometry [25]. Through an updated Lagrangian approach, NASTRAN calculates the linear strains in an updated coordinate system. This eliminates the effects of rigid body rotation [25].

NASTRAN solves a non-linear problem by dividing the total applied load into smaller increments. Each increment is solved through an updated stiffness matrix and updated element coordinates. NASTRAN solves for equilibrium at each load increment. The internal force:

$$F = \int_V \overline{B^T} s \, dV \tag{3-13}$$

depends upon the element matrix $\overline{B}$ which is part of the strain equation,

$$\{de\} = \left[\overline{B}\right]\{du\} \tag{3-14}$$

The $\overline{B}$ matrix can be divided into linear and non-linear parts:

$$\overline{B} = B_L + B_N \tag{3-15}$$

The x component elements of B_N are:

$$\begin{aligned} e_x &= \frac{\partial u}{\partial x} + \frac{1}{2}\left[\left(\frac{\partial u}{\partial x}\right)^2 + \left(\frac{\partial v}{\partial x}\right)^2 + \left(\frac{\partial w}{\partial x}\right)^2\right] \\ g_{xy} &= \frac{\partial u}{\partial y} + \frac{\partial v}{\partial x} + \left[\frac{\partial u}{\partial x}\frac{\partial u}{\partial y} + \frac{\partial v}{\partial x}\frac{\partial v}{\partial y} + \frac{\partial w}{\partial x}\frac{\partial w}{\partial y}\right] \end{aligned} \tag{3-16}$$

and the y and z component elements are similar. Differentiating equation 3-13 yields,

$$dF = \int_V \overline{B^T}(ds)dV + \int_V (d\overline{B^T}) s \, dV \tag{3-17}$$

This reduces to,

$$dF = \left[K_L + K_R + K_s\right]du \tag{3-18}$$

where

$$K_L = \int_V B_L^T D B_L \, dV$$
$$K_R = \int_V \left[B_L^T D B_N + B_N^T D B_N + B_N^T D B_L \right] dV \qquad \text{(3-19a,b,c)}$$
$$K_s = \int_V dB_N^T s \, dV$$

K_L represents the linear stiffness matrix. K_σ and K_R represent the geometric stiffness based on initial stress and the stiffness due to large rotations respectively. The geometric stiffness matrix is equivalent to the differential stiffness matrix used in buckling analysis [25].

Updating the stiffness matrix is the most time consuming process in the non-linear analysis. NASTRAN reduces the time required through adaptive algorithms. The algorithms converge to an equilibrium solution at each incremental load step and reduce the number of stiffness matrix updates required. NASTRAN contains several adaptive algorithms applicable to non-linear analysis, including a modified Newton-Raphson method as the default method [25]. From the linear solution,

$$\{F\} = [K]\{u\} \qquad \text{(3-20)}$$

the residual error vector of each iteration, i, is calculated from the internal force as,

$$\{R^{i+1}\} = \{P\} - \{F^i\} \qquad \text{(3-210)}$$

This residual error is carried into the next iteration to recalculate internal forces. The Newton-Raphson method converges when,

$$\left\| u^* - u^{i+1} \right\| \le q \left\| u^* - u^i \right\|^2 \qquad \text{(3-22)}$$

where q is a constant and u* is the true displacement. To achieve an equilibrium state, each load increment is converged to the true displacement. Once the increment is converged, the stiffness matrix is then updated.

NASTRAN has the ability to include follower forces in non-linear analysis. A follower force changes direction as the model deforms and rotates. Normally, forces maintain an orientation relative to the global coordinate system regardless of the deformation. In this study, follower forces were not included in the NASTRAN analysis. Aerodynamic pressure always acts normal to a lifting surface. Thus, as a wing deforms the pressure remains acting normal to the surface (i.e. a follower force). PanAir calculates the aerodynamic pressure distribution on the deformed wing surface. Therefore, the follower forces are developed within AVTIE and it is not required to develop them within NASTRAN.

Multiple Case, Non-Linear Fully Stressed Design

MATLAB code was developed to perform the fully stressed design algorithm for multiple load cases. First the code created individual non-linear input files for each load case. NASTRAN executed each input file and returned the element stresses. The MATALB code analyzed each element using the largest stress from all load cases. Each element was resized using equation 3-2. However, if the stress ratio $\sigma_i/\sigma_{allowable}$ was greater than one, the α was set to 0.9 and 0.2 if the stress ratio was less than one. Using a variable α allowed the optimization to add material quickly to alleviate overstressed elements and remove material slowly to avoid excessively thinning elements.

Once the elements were resized, the code created new input files for each load case including the new element thickness. These files were executed and the resulting element stresses were used in resizing. This process was repeated until the highest element stress was no more than 1.5% greater than the allowable stress.

Once the largest element stress was no more than 1.5% over the allowable stress, the α values were changed to 0.5 and 0.0 respectively. This new condition only added material to satisfy any stress violations, but did not remove material to achieve the absolute minimum weight. This prevented a tendency to diverge from the minimum weight design (see Figure 4-5). The resized model quickly satisfied the allowable stress limits. Once satisfied, the code exported element thickness and displacement files to AVTIE.

NASTRAN Buckling Analysis

A structure is buckled when an applied load causes an unlimited amount of deformation. In NASTRAN, adding the differential stiffness to the linear stiffness matrix leads to an eigenvalue problem that is solved for linear buckling [24]. The differential stiffness matrix is the first, higher-order terms in the strain/displacement relationship. The stiffness matrix for the model becomes:

$$[K] = [K_a] + [K_d] \tag{3-23}$$

In equilibrium, the total potential must be stationary.

$$\frac{\partial [U]}{\partial u_i} = [K_a]\{u\} + [K_d]\{u\} = 0 \tag{3-24}$$

This can be rewritten as:

$$\left([K_a] + P_a[\overline{K}_d]\right)\{u\} = 0 \tag{3-25}$$

where P_a is the applied load. This equation can be solved for the non-trivial values of P_a by:

$$\left|[K_a] + P_a[\overline{K}_d]\right| = 0 \tag{3-26}$$

The non-trivial values of P_a are the critical buckling loads. "The number of buckling loads obtainable…is equal to the number of degrees of freedom in the model"[24]. This implies,

$$l_i * P_a = P_{critical_i} \tag{3-27}$$

Equation 3-27 can be incorporated in equation 3-26:

$$\left|[Ka] + l_i[\overline{K}d]\right| = 0 \tag{3-28}$$

This is now an eigenvalue problem where the solutions of λ_i are scale factors of the applied load that cause a buckling condition. For a structure to be considered safe from buckling or buckling safe, the lowest value of λ_i should be greater than one. This implies that the structure will not buckle under the applied load P_a.

NASTRAN uses a Lanczos method to extract eignevalues for buckling analysis. This is a method similar to the inverse power method, but is more efficient. "This method computes accurate eigenvalues and eigenvectors" [24].

Trim for Rigid Aerodynamic Loads

For this joined-wing configuration, aircraft angle-of-attack and aft-wing flexible twist angle control pitch trim. Note that aft-wing twist only provides pitch trim control. Additional

control surfaces are used for roll control. The aft-wing is rotated at the wing root and remains rigid at the wing-joint. An un-modeled actuator in the vertical tail drives the twist angle. AVTIE uses a linear Taylor series approximation to compute a trimmed angle-of-attack a and aft-wing root twist angle d.

$$\begin{Bmatrix} C_L - C_{L0} \\ C_M - C_{M0} \end{Bmatrix} = \begin{bmatrix} \left(\frac{dC_L}{da}\right) & \left(\frac{dC_L}{dd}\right) \\ \left(\frac{dC_M}{da}\right) & \left(\frac{dC_M}{dd}\right) \end{bmatrix} \begin{Bmatrix} a - a_1 \\ d - d_0 \end{Bmatrix} \tag{3-29}$$

AVTIE then calls PanAir to regenerate the pressure distributions at the trimmed conditions. The researcher must pay special attention to the aft-wing root twist angle during the trimming process. A large angle-of-attack or twist angle will generate excessive drag and should be avoided if possible [4].

At selected points in the mission, PanAir trims the aircraft for a steady, pull-up or turn maneuver (2.5G load). This verifies the aircraft's ability to achieve maneuverable flight throughout the mission profile. L/D can be calculated at each of these points for future study. Most importantly, static stability requires that the center of gravity is forward of the aerodynamic center, and pitch trim requires that the center of gravity is at the center of pressure. Using the location of the payload mass to adjust the center of gravity at the end of the mission (zero fuel) aids the aircraft's ability to maintain a stable trim condition throughout the mission. This improves the aerodynamic performance at the trimmed condition by reducing the required angle-of-attack and twist angle. Equation 3-30 is used to calculate the necessary change in payload location to move

the center of gravity to the aerodynamic center. Once the payload mass is moved to an appropriate location, it is fixed at that location for the entire mission.

$$\left|X_{cg} - X_{ac}\right| \cdot \frac{TotalMass}{PayloadMass} = \Delta X_{cg} \tag{3-30}$$

Once the payload is fixed for trim at the end of the mission, the location of the fuel can be used at the beginning of the mission (maximum fuel load) to augment mass balancing of the aircraft. Adequate fuel management can be used to balance the center of gravity throughout the mission after initial conditions.

The connection of the forward and aft wings is considered to be a rigid joint. An un-modeled actuator assembly controls the twist of the aft-wing root. Twisting the aft-wing root for a trimmed condition generates additional structural stress in the aft-wing. AVTIE updates the finite element model with the enforced aft-wing twist required for trim. NASTRAN uses the aerodynamic loads and enforced twist of the trimmed condition to calculate deflections and optimize the structural design.

Trim for Flexible Aerodynamic Loads

Fully stressed design changes the overall weight and weight distribution of the sensor-craft. AVTIE recalculates the center of gravity location. AVTIE also recalculates the fuel required to complete the mission based on the Breguet range equation (3-1). Recall that the L/D ratio remains fixed in this study. The PanAir model is updated to account for the flexible deformation. PanAir generates new aerodynamic loads based on the deformed model. AVTIE uses these loads to re-trim the aircraft for a selected mission point using the same equilibrium

equations (3-29) as rigid trim. The center of gravity changes due to the optimized structural component thickness and updated fuel weight, so fuel management or payload mass balancing (3-30) may be needed.

Aerodynamic and Structural Optimization Process

Linear Optimization

Figure 3-5 illustrates the overall optimization process. The green boxes are functions performed by AVTIE. The lavender box highlights the PanAir function of generating flexible or rigid aerodynamic loads for a given angle of attack and twist. The blue box highlights the NASTRAN finite element structural optimization based on the aerodynamic loads and the geometric model.

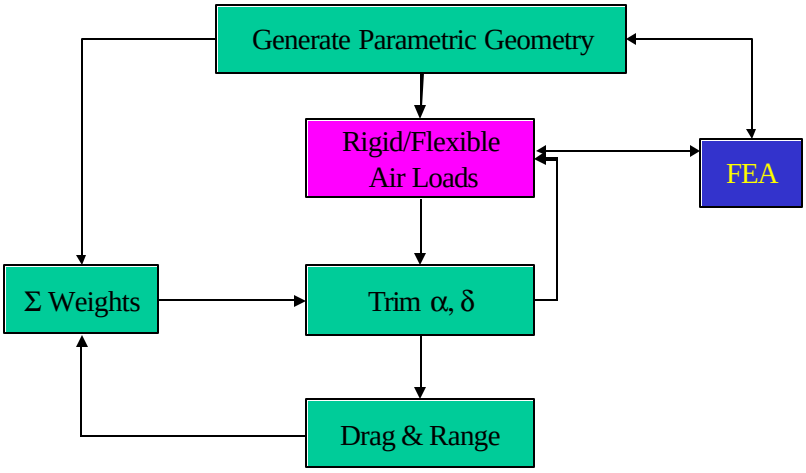

Figure 3-5. AVTIE Optimization Process

First, the default model is trimmed for a 2.5G maneuver using the undeformed model through seven points in the mission. At the end of the mission, the sensor-craft is trimmed for a 1.0G flight condition at 20,000ft. This is done for the cruise and design maneuvering speeds. The $\Delta\alpha$'s due to gust are then added into AVTIE and new aerodynamic loads are calculated in PanAir. These trimmed rigid aerodynamic loads, gust loads and inertia forces are transferred to NASTRAN through MATALB. The MATLAB code also creates taxi and landing impact loads by utilizing only scaled inertia forces at the beginning and end of mission conditions. NASTRAN performs linear fully stressed design to optimize the model for all the load cases. The new element thickness and displacement files are returned to AVTIE. The new weight of the vehicle is calculated in AVTIE. Also, a new total fuel requirement and center of gravity is calculated. AVTIE uses the displacement files for each mission point to incorporate the wing deformation into the PanAir model. New aerodynamic loads and stability derivatives are calculated and the model must be aerodynamically trimmed and mass balanced for all mission points. Also, the gust loads are recalculated using the 1.0G deformations and new element thickness. New $\Delta\alpha$'s are added to the 1.0G conditions. All the new load cases are again exported to NASTRAN through MATLAB, including the ground impact loads. Fully stressed design is performed to optimize the structure for the new loads. The deformations and element thicknesses are returned to AVTIE and the trim process is repeated for the new deformations, weights, and center of gravity. The process continues between flexible trim and linear fully stressed design until the weight changes by less than 2%. This optimal design is analyzed for global buckling through NASTRAN. A buckling load less than the design load (i.e., buckling eigenvalue of less than one) typically

indicates the onset of non-linear geometric effects. This implies the need to perform non-linear analysis and optimization.

Non-Linear Optimization

Beginning with the converged model from linear optimization, a final flexible trim is calculated using the linear deformations, optimized weight and center of gravity. The gust loads are again calculated. The trimmed aerodynamic loads, gust loads and impact loads are exported to NASTRAN through a MATLAB code which creates non-linear analysis files for each load case. The stresses from each load case are returned to MATLAB and the code resizes each element through the multiple case, fully stressed design algorithm discussed above. MATLAB and NASTRAN are executed repeatedly until the optimum design is achieved. MATLAB then creates and exports the element thickness and displacement files. AVTIE again performs flexible trim and gust load calculations. The non-linear fully stressed design and flexible trim processes are repeated until the weight changes by less than 2%. A final linear buckling analysis is performed for all mission points, gust loads, and impact loads.

The linear optimization and non-linear optimization processes are performed for the aluminum and composite models. Both models begin with the AVTIE, uniform thickness model. Results for both models are presented in Chapter 4.

Stochastic Analysis

The inboard, forward and aft-wings were modeled having normal Gaussian random material properties. The wing-joint was also modeled using a random material property. The

forward-wing was divided into two regions, the upper and lower surface, each having a separate random material property. The aft-wing was similarly divided into an upper and lower surface region defining two random material properties. The wing-joint skin elements all used a single random material property.

NASTRAN buckling analysis was executed using the five random material properties. The first buckling eigenvalue was computed for each analysis and a probability distribution function was generated. The process used was identical to the process developed by Choi, et al [27].

IV. Results

Joined-Wing Structure

The Sensor-Craft configuration optimized in this study performed similarly to the joined-wing results found by Wolkovich. When a vertical, distributed load was applied to the uniform thickness joined-wing model, the load caused a deformation in the vertical direction and the forward direction. Figure 4-1 depicts a plan view of the joined-wing under a vertical applied load. The wire-frame model is the undeformed shape.

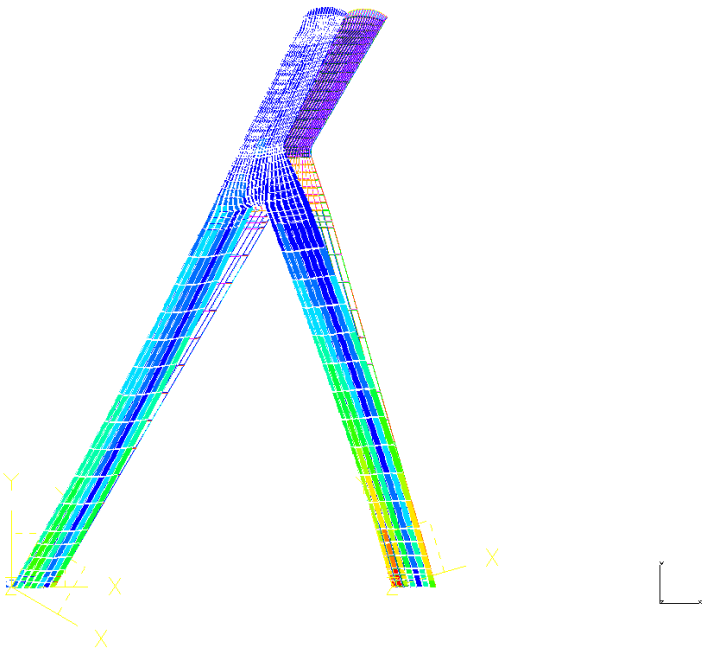

Figure 4-1. Uniform Thickness, Vertical Distributed Load

When the aft-wing is twisted, additional stresses and deformations occur. Figure 4-2 depicts the scaled deformation and Von Mises stress created by applying a -5.0º aft-wing twist. No aerodynamic or inertial loads were applied to the model.

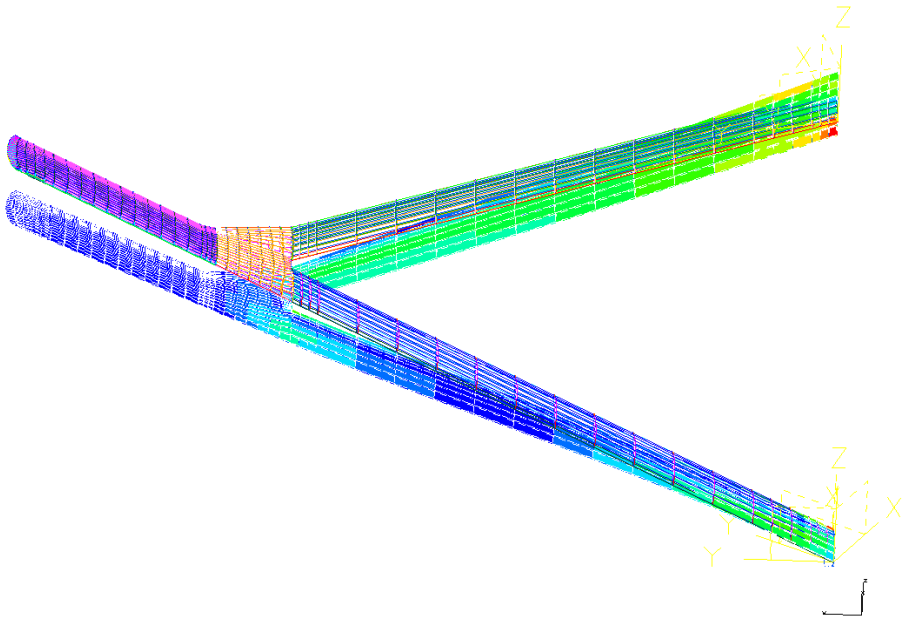

Figure 4-2. Uniform Thickness, -5.0º Aft-Wing Twist

Aerodynamic/Structural Coupling

This model exhibits closely coupled aerodynamic and structural behavior. Early in the analysis, a single mission point, 2.98 at 2.5G maneuver load was optimized using rigid and flexible trim. Also, the aft-wing jig shape was set to the trimmed aft-wing twist at each iteration. Table 4-1 lists the aerodynamic properties during the optimization process using rigid trim.

Iteration	Total Mass (kg)	Angle of Attack, α	Aft-Wing Twist, δ
0	14422	0.155	-1.453
1	10395	-1.066	-1.983
2	10540	-1.041	-1.890
3	10546	-1.041	-1.882
4	10545	-1.041	-1.882

Table 4-1. Rigid Trim, Linear Structural Optimization for Mission Point 2.98 at 2.5G Maneuver Load

This single load case optimized quickly without oscillation of the angle of attack and aft-wing twist. However, when the flexible aerodynamic trim was used, the aft-wing twist changed due to the structural weight change. In this single case optimization, the jig shape was set to –0.7°. Table 4-2 lists the same aerodynamic properties during the flexible trim and structural optimization and Figure 4-3 depicts a plot of the mass and twist angle at each iteration.

Iteration	Total Mass (kg)	Angle of Attack, α	Aft-Wing Twist, δ
0	14422	0.155	-1.453
1	10482	-1.066	-1.881
2	10414	-1.063	-1.980
3	10543	-1.060	-1.823
4	10423	-1.056	-1.996
5	10520	-1.057	-1.863
6	10431	-1.057	-1.985
7	10487	-1.059	-1.964

Table 4-2. Flexible Trim, Linear Structural Optimization for Mission Point 2.98, at 2.5G Maneuver Load and Jig Shape = -0.7°

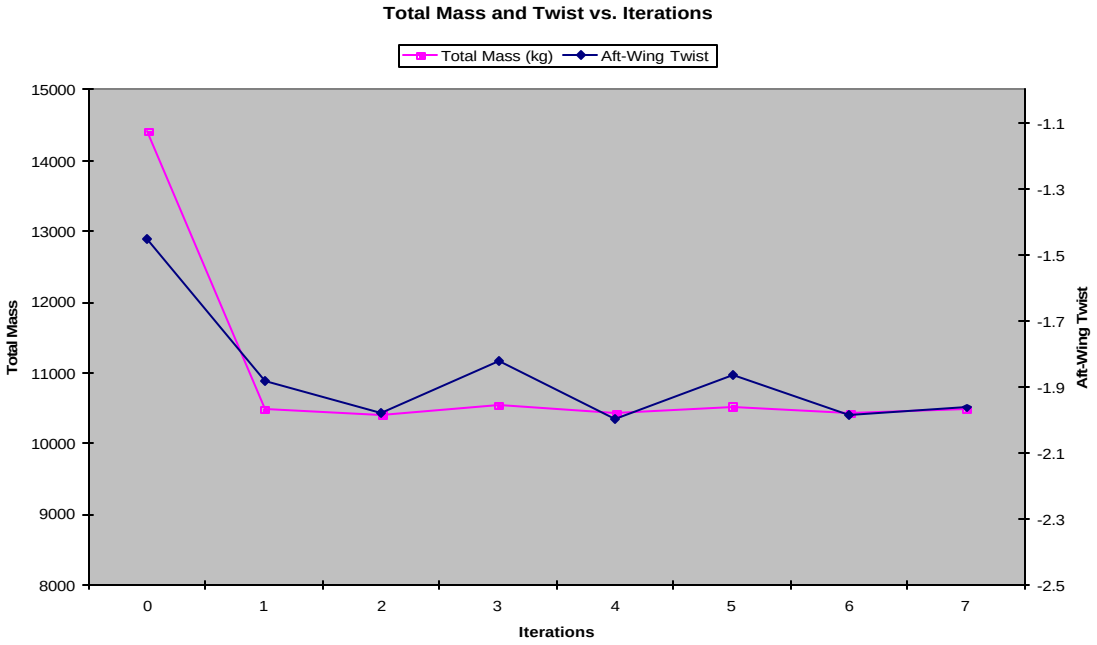

Figure 4-3. Total Mass and Aft-Wing Twist (d) versus Iterations

The angle of attack did not change significantly during the optimization process. In the aft-wing, the enforced twist added to the jig shape twist created additional stress in the aft-wing. The additional stress forced the fully stressed design to add mass to the aft-wing to relieve the additional stress. Once the mass was increased, the flexible trim process increased the twist (i.e., made the twist less negative) to create more lift. This relieved the stress in the aft-wing and the next optimization process reduced the structural mass. The reduced mass required a more negative twist angle, which again increased stress in the aft-wing. This single load case demonstrates the close interaction between aerodynamic trim and structural optimization.

Linear Aluminum Results

Initial optimization based on linear analysis of the aluminum model was performed using 2.5G maneuver loads at seven points in the mission. Taxi crater impact and landing loads were included. After three fully stressed design optimizations, the wing structure mass redistributed enough to cause the aircraft to be unable to achieve aerodynamic stability. The payload was moved forward in the fuselage (Equation 3-30) to provide an adequate center of gravity. Table 4-3 lists the wing structure and total vehicle mass after each NASTRAN structural optimization. Flexible aerodynamic trim was executed in AVTIE after each structural optimization. The total fuel required was not recalculated after each structural optimization.

Iteration	Wing Structure (kg)	Gross Take-Off (kg)
0	6779	39034
1	2738	34992
2	4079	36333
3	4129	36383
4	3786	36041
5	3766	36020

Table 4-3. Optimized Mass at Structural Iterations 2.5G Maneuver, Taxi, and Landing (No Gust Loads)

The aluminum model converged to within 1.0% change in the structural mass. Figures 4-4 and 4-5 depict the upper and lower wing skin thickness distributions. As described by Wolkovich, the structural mass becomes concentrated at the upper leading edge and lower trailing edge of the wing box [10]. In the substructure of the aft-wing (Figure 4-6), the aft-most spar increased in thickness as well. The wing root substructure remained at minimum gage thickness. This is an indication that the bending stress carried by the wing skin is greater than the shear

stresses carried by the spars. The other ribs and spars also remained at minimum gage thickness. This material distribution places the majority of the mass at the maximum perpendicular distance from the neutral surface. The neutral surface is aligned with the joined-wing plane as illustrated in Figure 2-1.

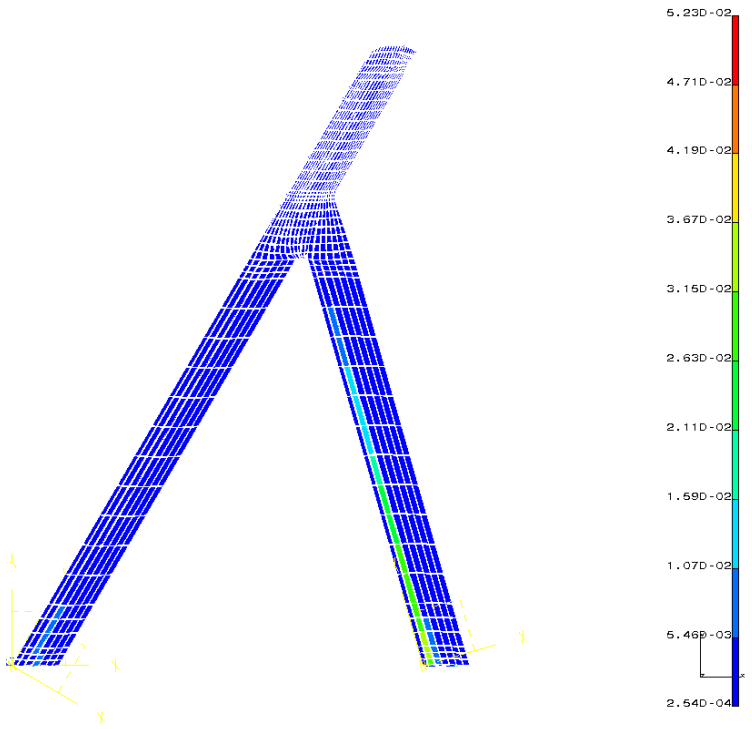

Figure 4-4. Linear Optimized Joined-Wing Skin Thickness Distribution, Top Surface

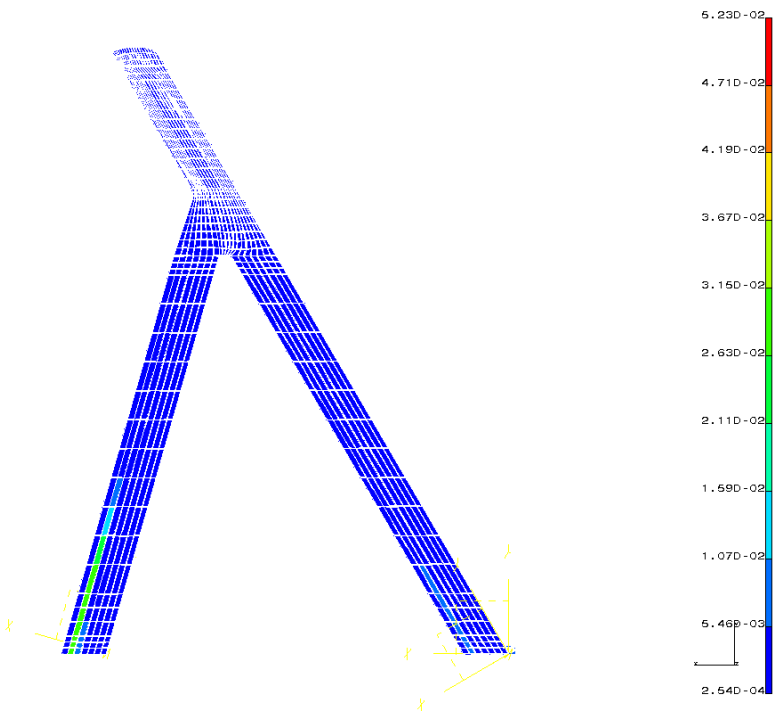

Figure 4-5. Linear Optimized Joined-Wing Skin Thickness Distribution, Lower Surface

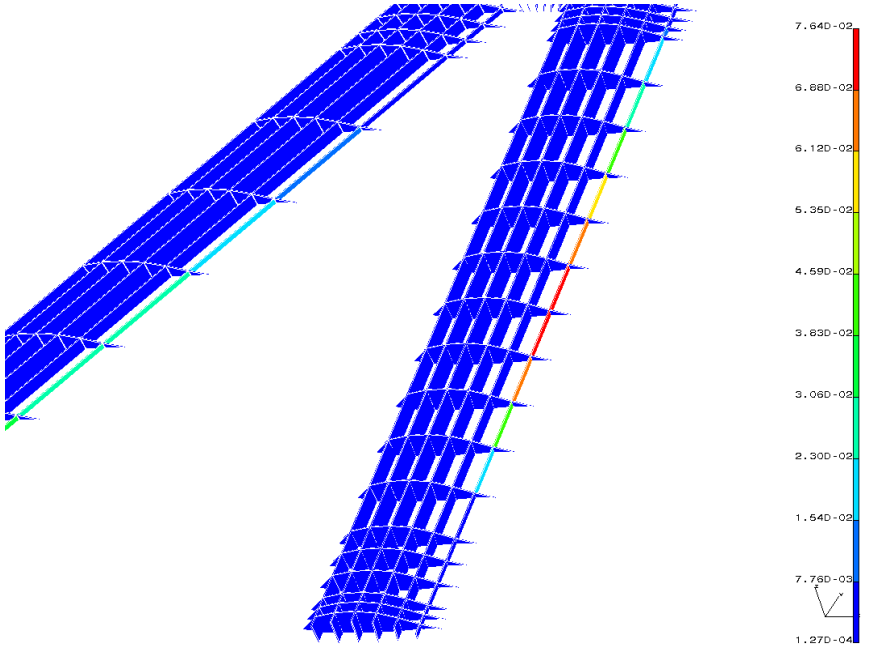

Figure 4-6. Linear Optimized Aft-Wing Substructure Thickness

A buckling analysis was performed for all optimized load cases. The critical buckling eigenvalue of 0.85 occurred at the taxi crater-impact load case. The most severe buckling occurred in the forward-wing. All flight conditions exhibited a buckling eigenvalue of 1.2 or greater. Gust loads were developed for the 2.98 mission point at 20,000ft. Buckling analysis was also performed for these gust loads. Buckling occurred at the cruise and maneuver speed gust conditions with eigenvalues of 0.64 and 0.75 respectively. This indicated that the critical aerodynamic load cases were gust conditions and should be added to the optimization process.

A second linear optimization process incorporated the critical end-of-mission gust loads. It also updated the fuel requirement according to the Breguet range equation after each structural optimization. It also reduced the minimum gage thickness of the outboard spars to more accurately reflect the required material. All load cases, including taxi and landing, were included from the initial iteration. Also, the payload mass was placed at the location required by the mass balancing for dynamic stability from the previous linear optimization method. NASTRAN was unable to converge the multiple load case model in a single optimization analysis when gust loads were included. The NASTRAN analysis was restarted from the final element thickness values, and the step size (i.e., α value in Eq. 3-9) was reduced. This restart with a reduced α improved the optimization performance and reduced the stress constraint violation to less than 1.5% violated. Table 4-4 lists the optimized mass at each iteration.

Iteration	Wing Structure (kg)	Gross Take-Off (kg)	Total Fuel Required (kg)

0	6779	39034	24674
1	6113	37491	23756
2	5485	36075	23226
3	5312	35409	22679
4	5282	35369	22659

Table 4-4. Optimized Mass at Structural Iterations (Including Gust Load Cases, Updated Fuel Requirement)

This revised optimization process reflects an aluminum joined-wing structure that is designed for minimum weight. Also, as the wing structure mass decreased, the total fuel requirement and total weight decreased.

Buckling analysis was performed on the optimized model for all load cases. The critical buckling eigenvalues for all 2.5G flight conditions were above 1.25. The lowest buckling values for maneuver loads (1.257, 1.274, and 1.300) do not meet the 50% factor of safety requirement. The gust load cases exhibited buckling eigenvalues of 0.63 for cruise and 0.55 for design maneuvering speed at the end of the mission. The taxi and landing impact buckling eigenvalues were 1.09 and 5.16 respectively. Figure 4-7 depicts the first buckling mode shape of the maneuver gust condition.

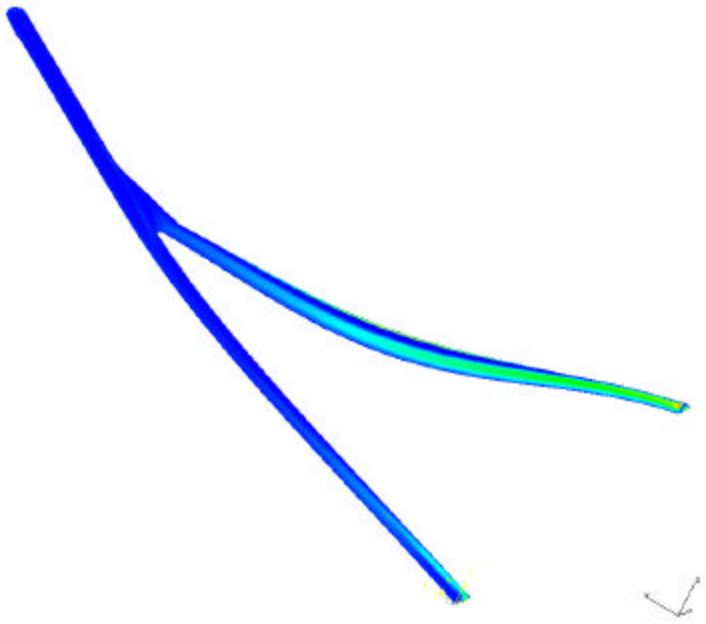

Figure 4-7. First Buckling Mode Shape, 2.98 Gust at Maneuver Speed

The gust condition induced a 3.03º and 4.23º change in angle of attack for the cruise and maneuver gust respectively (Equation 3-4). The gust alleviation factor for the optimized mass was 54% (Equations 3-7 and 3-8). These gust loads increased the load factors by 3.06G and 3.16G for cruise and maneuver speeds (Equation 3-6). Figure 4-8 depicts the first buckling mode shape of the taxi impact condition. In this load case, the forward-wing buckles first. It also buckles in a downward mode shape. This is not intuitive since a down load would cause tension in the upper wing surface and compression in the lower wing surface. However, the down load is a distributed load along the span of the forward and aft-wings due mainly to the weight of the fuel carried in the wing. Thus, a large portion of the load is carried in the forward-wing inboard of the wing-joint.

This downward load inboard of the wing-joint causes the downward deflection and buckling of the forward-wing.

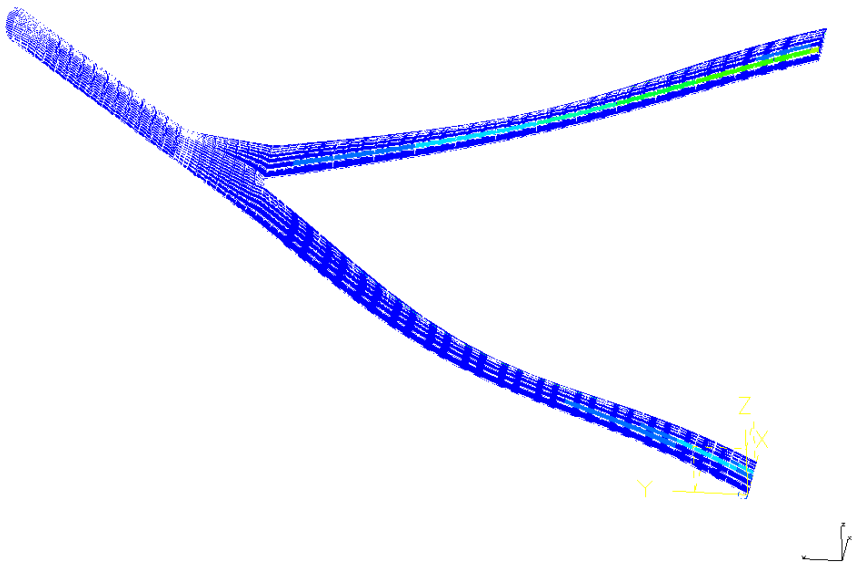

Figure 4-8. First Buckling Mode Shape, Taxi Impact Load

Non-Linear Aluminum Results

Once the aluminum model was optimized and trimmed, a non-linear static analysis was performed on a single 2.5G steady maneuver load case at the beginning of the mission. The buckling eigenvalue for this case was 1.76. This non-linear analysis significantly differed from the linear NASTRAN output. The wing tip deflection for a maneuver load case was calculated through linear analysis to be 3.24 m. The non-linear analysis calculated the tip deflection for the same load case as 18.08 m. Figure 4-9 displays the linear and non-linear deformations of a single load case.

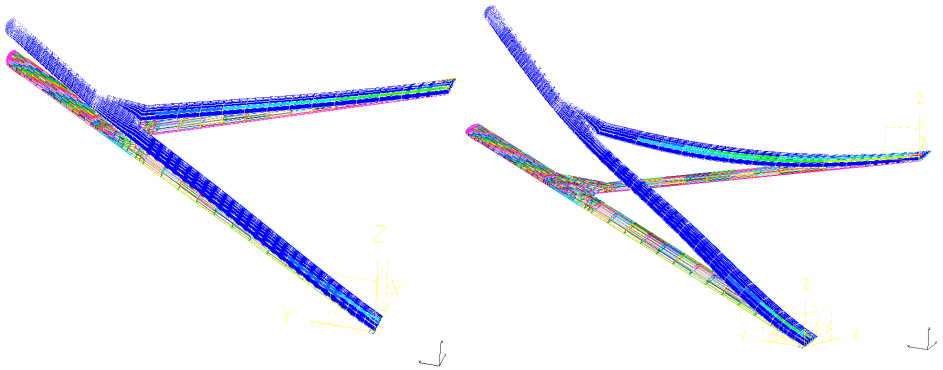

Figure 4-9. Linear and Non-Linear Structural Deformations, 2.5G Maneuver Load, Beginning of Ingress

Figure 4-10 displays a graph of the incremental load versus the wing tip deflection for non-linear analysis of a 2.5G steady maneuver. This graph displays an expected nearly linear slope up to approximately 70% of the 2.5G applied load. Above 70%, the structure appears to soften and deflections increase rapidly as load is increased. This highlights that geometric non-linearity is present in the joined-wing model well below the buckling eigenvalue at ~4.5G load factor. .

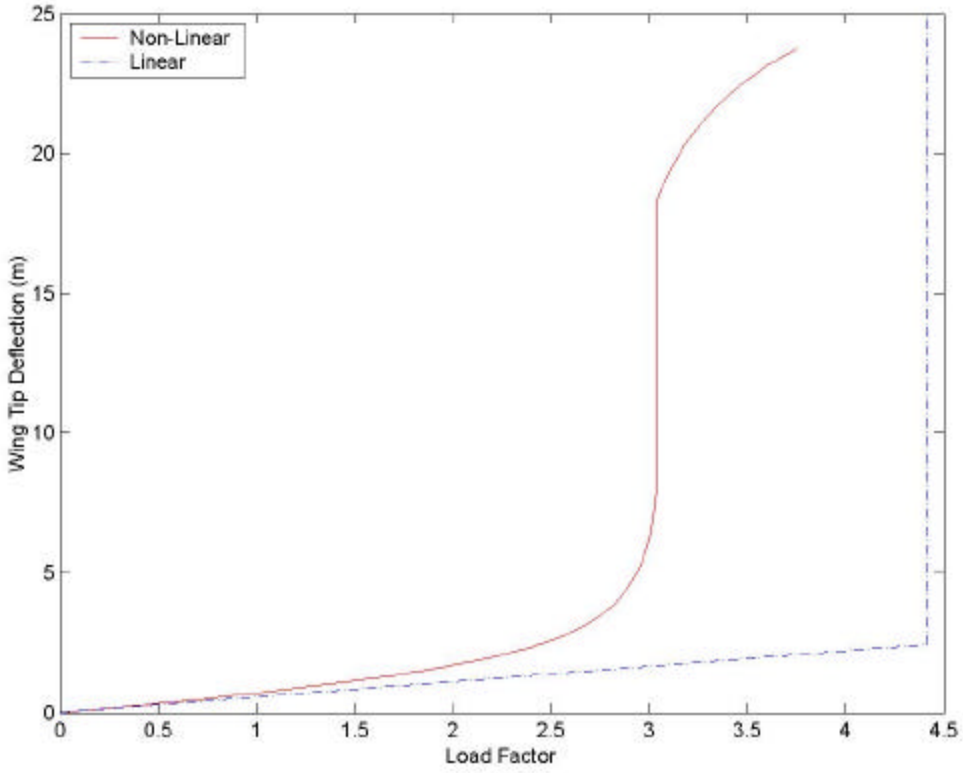

Figure 4-10. Load Factor vs. Wing Tip Deflection, 1.00 at 2.5G Maneuver

Figure 4-11 depicts the non-linear and linear wing-tip deflection versus load factor for a gust load at maneuver speed. In this case the critical buckling eigenvalue (? = 0.55) was less than the linear design load factor. However, the critical buckling eigenvalue was approximated by the non-linear analysis at the point of reflex on the non-linear curve.

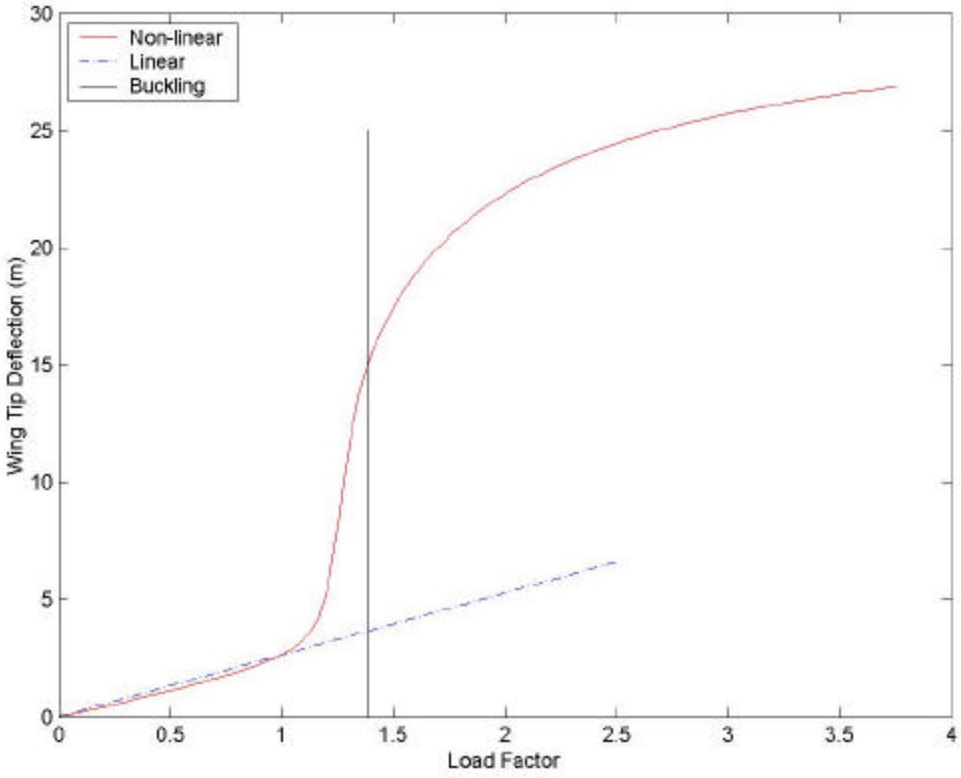

Figure 4-11. Load Factor vs. Wing Tip Deflection, 2.98 Gust at Maneuver Speed

The non-linear stress ratio algorithm for a multiple load case did not converge for a fixed step size as in (Equation 3-9). The mass reduced towards a converged solution and then diverged (Figure 4-12).

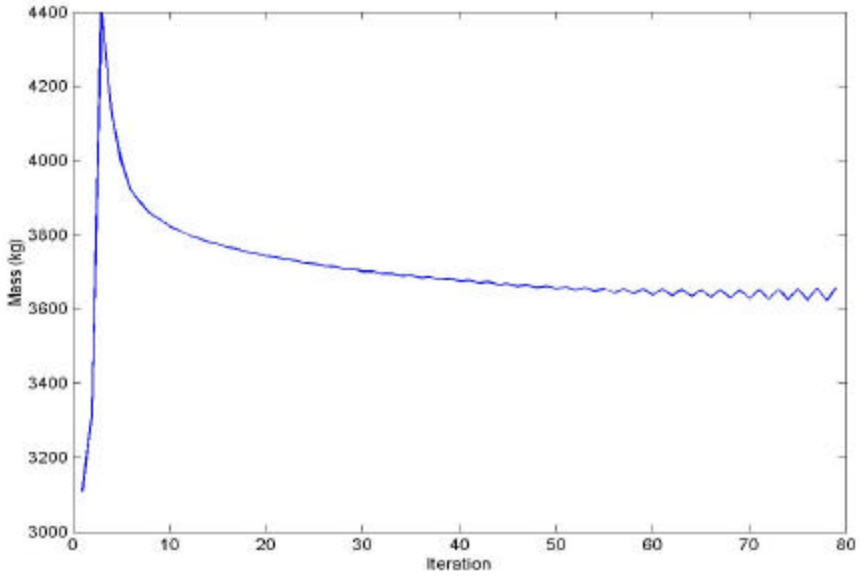

Figure 4-12. Non-Linear FSD Iterations versus Mass

An adaptive condition was added to the MATLAB fully stressed design algorithm. Once the stress constraint violation reduced to less than 1.5%, the a value was set so that material was only added to the elements and not removed. This algorithm does not produce a minimum weight design, rather it produces a design that satisfies the stress constraints and approaches a minimum weight. An example of the adaptive non-linear iterations versus wing structure mass is plotted in Figure 4-13.

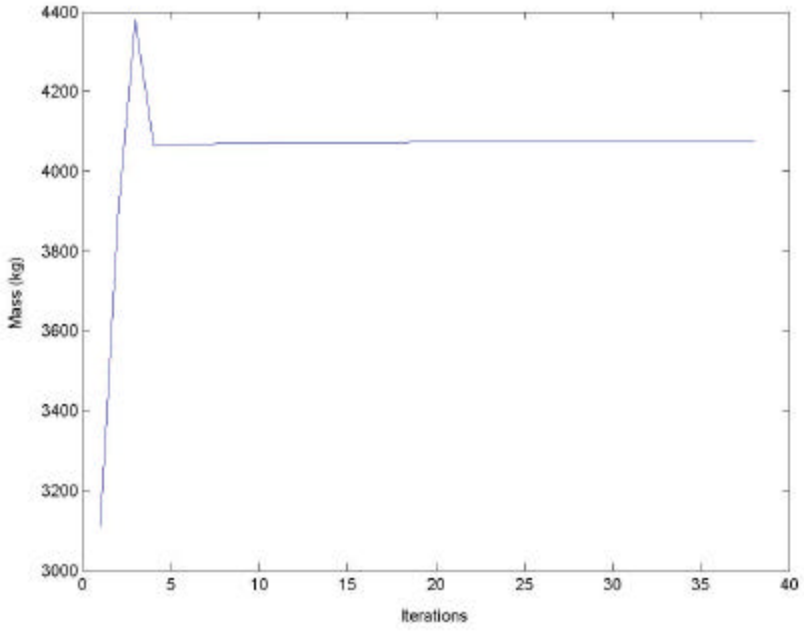

Figure 4-13. Adaptive Non-Linear FSD Iterations versus Mass

The adaptive method produced the optimized mass listed below in Table 4-5.

Iteration	Wing Structure (kg)	Gross Take-Off (kg)	Total Fuel Required (kg)
0	5282	35379	22797
1	7378	43346	27907
2	8020	45810	29493
3	8595	48008	30909
4	9502	51478	33142
5	9804	52628	33883
6	9800	52616	33875

Table 4-5. Non-Linear Optimized Mass at Structural Iterations (All Load Cases, Updated Fuel Requirement)

The non-linear optimized mass was significantly higher than the linear optimization predicted. A buckling analysis was performed on the optimized model for all mission cases. The critical buckling cases were taxi impact and gust maneuver conditions with buckling eigenvalues of 1.122 and 1.410 respectively. All flight load cases were buckling safe with the lowest eigenvalue of

2.840. The buckling mode shapes of the critical cases were similar to the buckling shape of the linear optimization model (Figures 4-7 and 4-8).

The material distribution was also similar to the linear model, however the thickness of each element was approximately 50% higher. Figures 4-14 and 4-15 display the element thickness distribution of the top skin surface and the aft-wing substructure respectively.

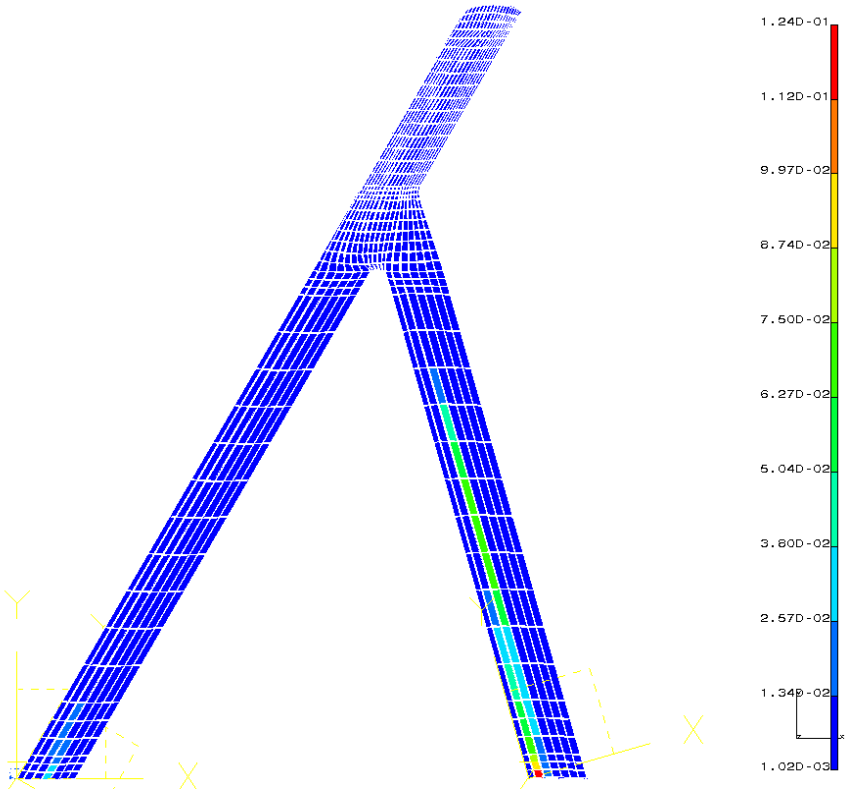

Figure 4-14. Non-linear Optimized Joined-Wing Skin Thickness Distribution, Top Surface

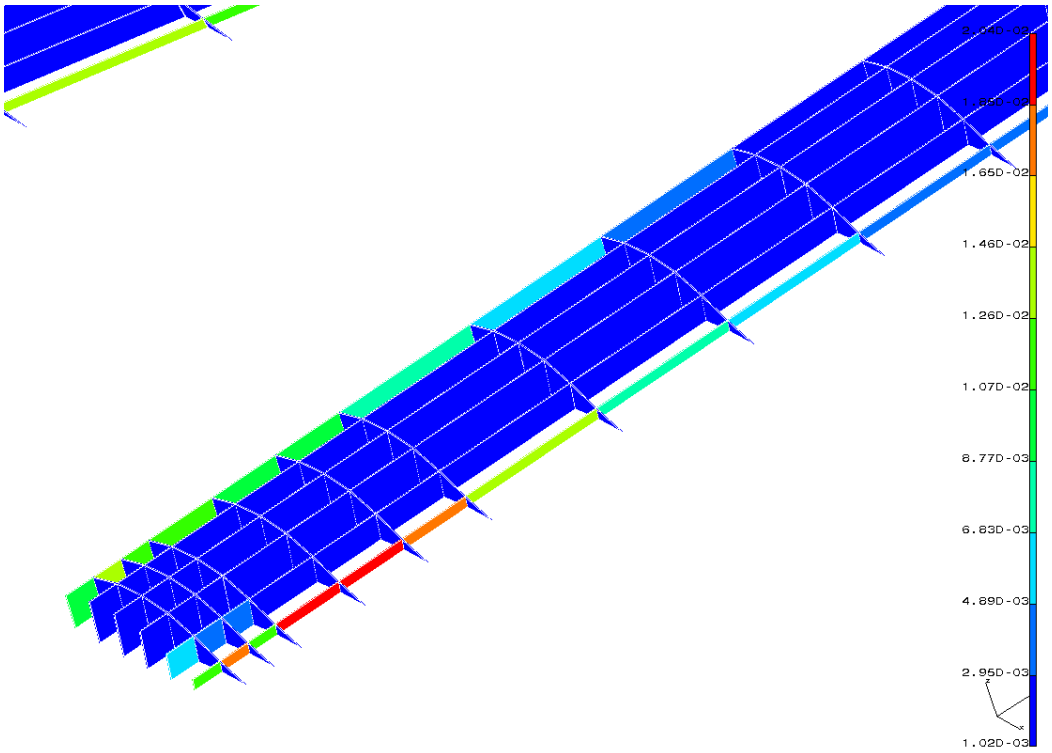

Figure 4-15. Non-linear Optimized Aft-Wing Substructure Thickness

Linear Composite Results

The composite model was optimized starting from the AVTIE-generated, uniform thickness model. Aerodynamic loads and trim conditions were created for the default model and MATLAB was used to transform this model into a CLAS material and graphite/epoxy, composite model. The maximum allowable fiber strain was used as the design criteria in the NASTRAN fully stressed design algorithm. The use of composite materials reduced the required mass. This, in turn, reduced the total fuel requirement. Table 4-6 displays the initial linear optimization iteration.

Iteration	Wing Structure (kg)	Gross Take-Off (kg)	Total Fuel Required (kg)
0	6779	39034	24674
1	4166	34332	22103

Table 4-6. Composite, First Fully Stressed Design, Linear Analysis (All Load Cases, Updated Fuel Requirement)

The first structural optimization reduced the non-CLAS material to minimum gage thickness. The CLAS material was thickened at the aft-wing root in a manner similar to the aluminum model. The upper-leading and lower-trailing edges were thickened (Figures 4-16 and 4-17). Since only the graphite/epoxy plies in the CLAS material were thickened, the increase in total element thickness of the CLAS material was minimal.

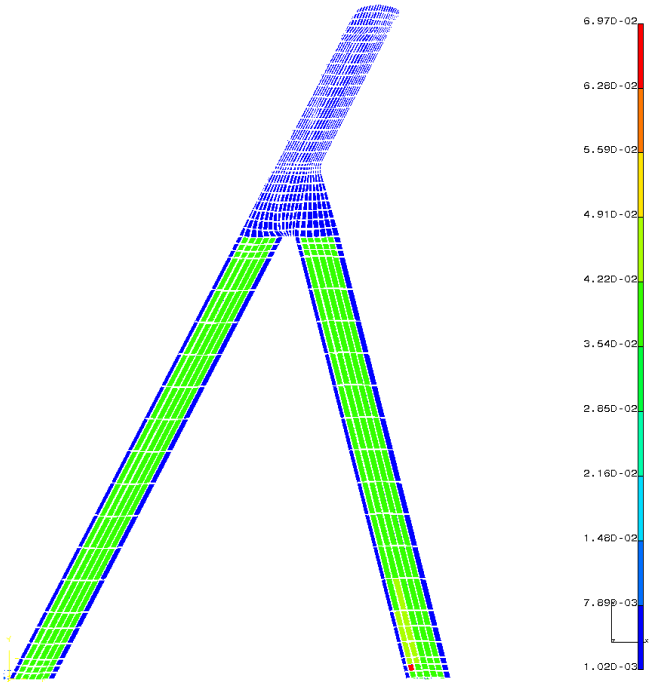

Figure 4-16. Composite, Linear Optimization Joined-Wing Skin Thickness Distribution, Top Surface, First Structural Iteration

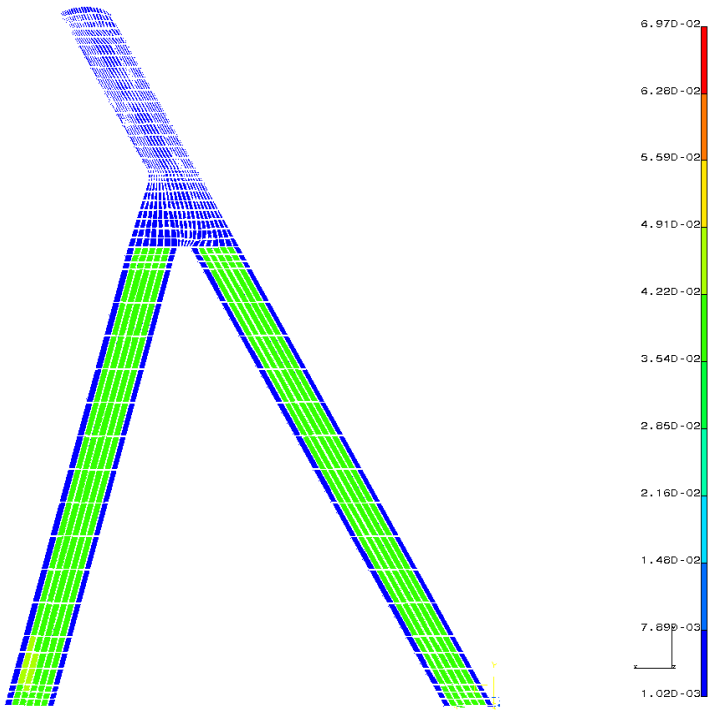

Figure 4-17. Composite, Linear Optimization Joined-Wing Skin Thickness Distribution, Lower Surface, First Structural Iteration

The buckling mode shape was analyzed for the gust load condition at maneuver speed for this first structural optimization iteration. The first buckling mode occurred at an eigenvalue of 1.14. Figure 4-18 depicts the shape of this buckling mode. This indicates that the initial structural optimization created a buckling-safe design.

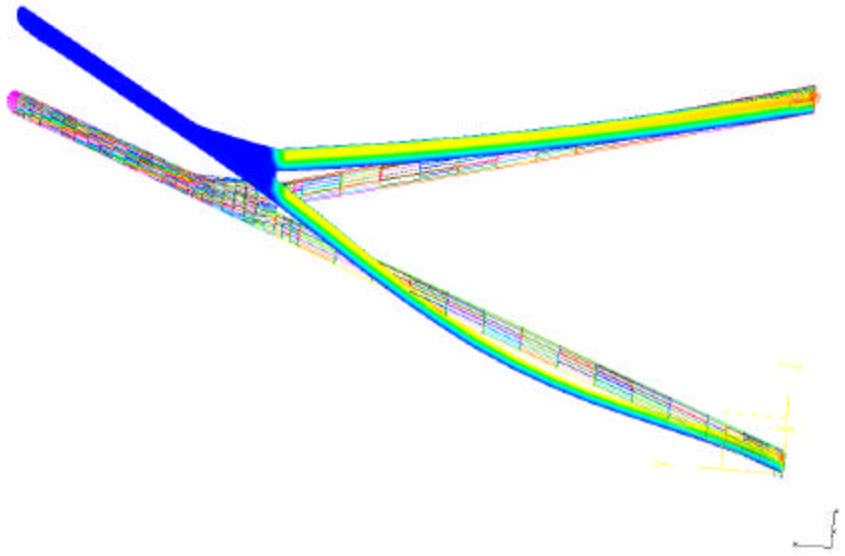

Figure 4-18. Composite, First Buckling Mode Shape, 2.98 Gust at Maneuver Speed

In this buckling case, the forward-wing buckled before the aft-wing. However, the aerodynamic loads and inertia loads applied to the model were loads developed for the uniform thickness aluminum model. The model is not in aerodynamic trim for the new mass distribution. These factors increased the compressive stress in the forward-wing and caused the buckling.

Stochastic Results

An initial stochastic analysis was performed using the linear optimized aluminum model and the taxi crater impact load case that was 9.0% buckling safe. A Gaussian normal random variable was applied to five regions within the wing structure to model uncertainties within the material properties. The standard deviation of the material random variables was 20% with a mean value of the Young's modulus for aluminum (Table 3-3). One thousand analysis cases were

run and created a normal probability distribution function of the output. The mean of the output was 1.09 and the standard deviation was approximately 10% (Figure 4-19).

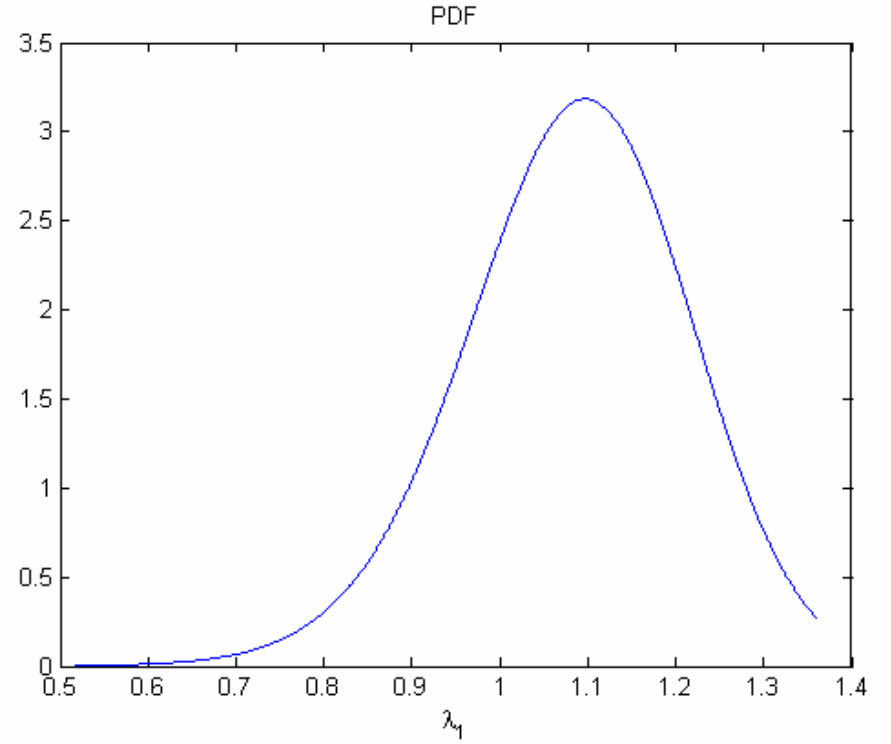

Figure 4-19. Probability Distribution Function, Aluminum Model, Near-Buckling Load Case

Also, a cumulative distribution function was generated. This predicted an 18% probability of failure at a limit state of 1.0. This indicated that the randomness in the material was 18% likely to cause failure at the applied load. Figure 4-20 depicts the cumulative distribution function.

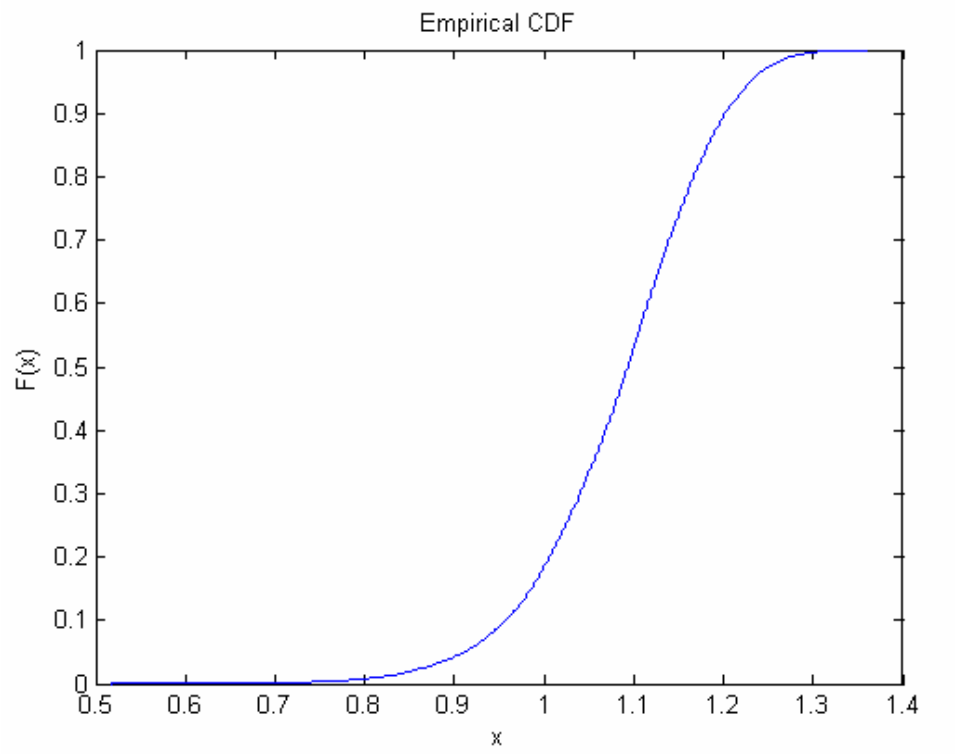

Figure 4-20. Cumulative Distribution Function, Aluminum Model, Near-Buckling Load Case

V. Conclusions and Recommendations

Aerodynamic and Structural Coupling

This study demonstrated that this proposed sensor-craft configuration is a highly coupled, multi-disciplinary design. The aerodynamic loads depend on the deformation of the structure. As the joined-wing deforms the direction of the aerodynamic loads changes due to the deformation. Because of this change in direction the lift component of the aerodynamic pressure vector is altered. To maintain the same magnitude of the lift component, the angle of attack must change. This creates an overall change in the pressure distribution of the wing. The new aerodynamic load creates a new deformation of the joined-wing. The new deformation creates a different stress distribution within the joined-wing structure. The structural optimization process changes the material thicknesses to prevent an overstress condition. This changes the overall weight of the sensor-craft.

The updated weight drives another change in the aerodynamic load requirements. Also, as the weight varies, the total fuel required varies. A change in fuel weight also changes the aerodynamic load requirements throughout the mission. Any change in aerodynamic loads affects the aerodynamic stability and trim of the sensor-craft.

As the aerodynamic loads change due to deformation and mass variances, the trim condition for the sensor-craft also must change. To meet the requirement for a new aerodynamic load the angle of attack and the aft-wing twist angle will change. Because the twist of the aft-wing is an enforced twist from a manufactured shape, the twisting of the aft-wing generates additional stresses in the configuration. This additional stress drives the structural optimization process to

change the material distribution to meet the allowable stress requirements. The redistribution of mass affects the center of gravity of the vehicle. This change of the center of gravity affects the overall mass balancing of the sensor-craft. The payload location can be adjusted (Equation 3-30) to relocate the center of gravity to a more favorable location.

In this sensor-craft configuration, a change in deformation, weight, fuel required, angle of attack, aft-wing twist angle or payload location will affect the aerodynamic and structural characteristics of the vehicle. Any change in the aerodynamic loads also has repercussions in trim, structural optimization, mass balancing, and structural deformation. This model demonstrates the highly coupled nature of a joined-wing configuration.

Non-Linear Analysis

Linear structural optimization of the aluminum model created a buckling safe design for all maneuver loads not including gust or ground impact loads. Buckling is typically the first indication of non-linearity in the model. However, as shown in Figure 4-7, the non-linear effects occur at a much lower load factor than the buckling load. Although for the gust conditions, the buckling eigenvalue predicts a slightly higher onset of non-linear effects than the actual non-linear analysis (Figure 4-11). Buckling is caused by compression. The load applied to the joined-wing causes bending stresses in the forward and aft-wings. The bending stress of the forward-wing is partially relieved through compression of the aft-wing. The high buckling eigenvalues for the 2.5G maneuver loads indicate that a large bending stress must be applied to develop sufficient compression in the aft-wing to cause buckling. The large bending stress is most likely the cause of the non-linearity in the joined-wing configuration. Thus, buckling analysis of an optimized, linear

fully stressed design is insufficient to predict the onset of non-linear effects in this joined-wing configuration.

Non-linear analysis predicts a much higher deformation than the linear analysis for the aluminum model. The larger deformations produce correspondingly larger stresses. This drives the fully stressed design algorithm (Equation 3-9) to increase the element thicknesses to meet the allowable stress constraints. Thus, the overall weight increases when non-linear analysis is included in the design optimization process. For a large span, joined-wing configuration such as sensor-craft, non-linear analysis is critical to accurately capture the large deformations and stresses.

Joined-Wing Structural Analysis

A joined-wing structure can not be intuitively analyzed. Due to the offset of the aft-wing in the x and z directions, a load applied in the vertical direction will cause a deformation of the structure in the positive z direction and the negative x direction. This forward bending of the joined-wing is due to the plane of bending not being aligned with the x-y plane. The plane of bending is aligned with the plane of the joined-wing structure (Figure 2-1).

Also, the optimal design of the joined-wing box structure is not a uniform thickness cross-section. The mass should be placed as far away from the inclined plane of bending as possible. This requirement leads to the thickening of the upper leading edge and lower trailing edge (Figure 2-2).

AVTIE Recommendations

The design philosophy of AVTIE has led to the creation of a very useful tool in analyzing a multi-disciplinary problem. However, AVTIE contains limitations due to the software design. Currently AVTIE can not produce a structural analysis model other than the uniform thickness, aluminum model. AVTIE must contain the ability to generate a distributed-thickness, multiple-material structural model. The designer should be able to designate materials for individual elements or a range of elements. In addition, AVTIE must allow the user to select linear static, non-linear static, linear fully stressed design, or non-linear fully stressed design as the NASTRAN analysis method. Finally, for future studies with this program, AVTIE should automatically perform aerodynamic trim and structural optimization iterations from a user defined model and flight conditions.

A final recommendation is to re-write AVTIE into a software language more widely used. Adaptive Modeling Language is not intuitive and has a steep learning curve associated with it. Also, the de-bugging and error message generator available in AML is unhelpful. Thus, correcting errors in the object-oriented code becomes difficult in a very large program such as AVTIE.

Model Recommendations

The structural model can be reduced to a two-spar design to reduce the redundant structure and the NASTRAN analysis time required. Also, the number of ribs in the forward and aft-wings can be reduced. This will produce a more realistic model of the sensor-craft

configuration. A dynamic analysis of the landing and taxi impact loads should be performed to obtain an accurate applied load.

Recommendations for Future Study

This highly coupled sensor-craft model can be geometrically optimized. Variables such as wing sweep, joint-location, aft-wing x- and z-offset, and aft-wing dihedral can be varied to determine and optimum geometric configuration that is aerodynamically stable, mass balanced, buckling safe, and a minimum weight design. Future studies can also quantify the sensitivities of the coupling effects. This would provide a method of estimation for future joined-wing optimization studies.

Appendix A:

AVTIE Interface and Configuration Files

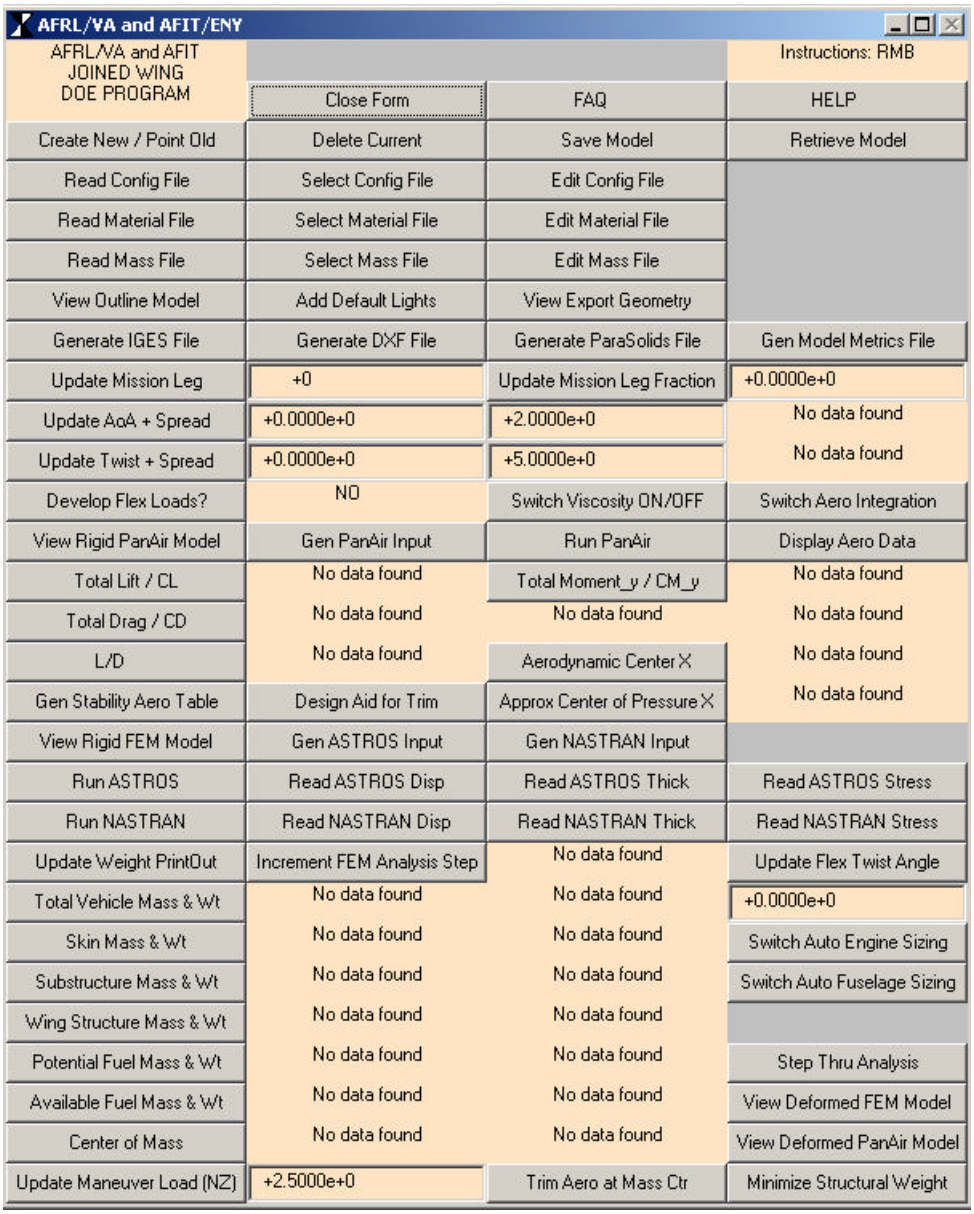

Figure A-1. AVTIE User Interface Menu

Baseline-Configuration-V01.txt

```
LABEL                                    BASELINE JOINED-
WING V03 - 100 foot length (vhf) 360 degree view (metric
units)

IB-SWEEP                                 30.0 DEG
OB-SWEEP                                 30.0 DEG

FUSELAGE-LENGTH                            30.0    M
(controls mass model)

FORWARD-FUSELAGE-WIDTH                   1.25 M
IB-SPAN                                  22.0 M
JOINT-SPAN                                    4.0  M
OB-SPAN                                  6.25 M
WING-TIP-SPAN                            1.75 M

IB-FORE-DIHEDRAL                         9.0  DEG
OB-DIHEDRAL                              9.0  DEG
JOINT-DIHEDRAL                           9.0  DEG

AFT-ROOT-OFFSET-X                        22.0 M
AFT-ROOT-OFFSET-Z                        7.0  M

IB-FORE-WING-IB-CHORD                    2.5  M
IB-AFT-WING-IB-CHORD                          2.5  M
IB-FORE-WING-OB-CHORD                    2.5  M
IB-AFT-WING-OB-CHORD                          2.5  M
FORE-AFT-OFFSET-AT-JOINT                      0.625     M
WING-MERGE-SMOOTHNESS-FACTOR                    3
(0.5<WING-MERGE-SMOOTHNESS-FACTOR<3)
OB-WING-IB-CHORD                         2.5  M
OB-WING-OB-CHORD                         2.5  M
IB-FORE-WING-IB-TWIST                    0.0  DEG
IB-FORE-WING-OB-TWIST                    0.0  DEG
IB-AFT-WING-IB-TWIST                          0.0  DEG
OB-WING-OB-TWIST                         0.0  DEG

GLOBAL-AIRFOIL                           LRN-1015.txt
fx-60-126-1.txt

IB-FORE-WING-IB-AIRFOIL-THICKNESS        1.0  NO-DIM
IB-FORE-WING-OB-AIRFOIL-THICKNESS        1.0  NO-DIM
IB-AFT-WING-IB-AIRFOIL-THICKNESS         1.0  NO-DIM
IB-AFT-WING-OB-AIRFOIL-THICKNESS         1.0  NO-DIM
```

```
OB-WING-IB-AIRFOIL-THICKNESS          1.0  NO-DIM
OB-WING-OB-AIRFOIL-THICKNESS          1.0  NO-DIM

FEM-SPAN-PARTITIONS                   4 4 12 4 8 4 12
FEM-CHORD-PARTITIONS                       8 6 8

AERO-SPAN-PARTITIONS                       2 2  6 2 7 2 12
AERO-CHORD-PARTITIONS                 10 6 10

SURFACE-SPAN-PARTITIONS               2 2 12 2 4 2 12
SURFACE-CHORD-PARTITIONS                   4 3 4

END
```

Baseline-Weights-V02.txt

LABEL BASELINE JOINED-WING V03 - 100 foot length (vhf) 360 degree view (metric units)

ACCELERATION-DUE-TO-GRAVITY	9.8	M/S^2 (USED TO CONVERT BETWEEN MASS AND WEIGHT)
DEFAULT-STRUCTURAL-ELEMENT-THICKNESS	2.54e-03	M
ENGINE-LOCATION-X	nil	M (TBD)
ENGINE-LOCATION-Z	0.0	M (TBD)
FUSELAGE-BLACK-BOX-MASS	3550.1	KG (TBD)
FUSELAGE-BLACK-BOX-LOCATION-X	-2.0	M (TBD)
FUSELAGE-BLACK-BOX-LOCATION-Z	1.0	M (TBD)
FUSELAGE-STRUCTURE-LOCATION-X	25.0	M (TBD)
FUSELAGE-STRUCTURE-LOCATION-Z	0.0	M (TBD)
VERTICAL-TAIL-STRUCTURE-MASS	100.0	KG (TBD)
VERTICAL-TAIL-STRUCTURE-LOCATION-X	nil	M (TBD)
VERTICAL-TAIL-STRUCTURE-LOCATION-Z	nil	M (TBD)
FUEL-DENSITY	810.0	kg/m^3 for kerosene
FUEL-FUSELAGE-MASS	0.0	KG (TBD)
FUEL-FUSELAGE-LOCATION-X	nil	M (TBD)
FUEL-FUSELAGE-LOCATION-Z	nil	M (TBD)

WING-STRUCTURE-MASS-IN-MISSION 7680 KG (first estimate and then update as real wing weight is recursively converged)
END

Aluminum-Metric.txt

LABEL BASELINE JOINED-WING V03 - 100 foot length (vhf) 360 degree view (metric units)

MATERIAL-E11	7.240e+10	Pa
MATERIAL-E66	2.758e+10	Pa
MATERIAL-DENSITY	2768.0	kg/m^3
MATERIAL-STRESS-TENSION-ALLOWABLE	1.034e+08	Pa
MATERIAL-STRESS-COMPRESSION-ALLOWABLE	1.034e+08	Pa
MATERIAL-STRESS-SHEAR-ALLOWABLE	5.516e+07	Pa

END

Appendix B:

AVTIE Procedures

Mouse buttons are defined as:

[LMB]: Left Mouse Button
[MMB]: Middle Mouse Button

[RMB]**: Right Mouse Button**

AVTIE Initial Rigid Trim Process

1. Open AML 3.3 from the desktop. [LMB] **OK**
2. [LMB] **My AML Utilities**
3. [LMB] **LOAD AVTIE**. Wait for AML Editor Window message: **AVTIE Loaded!**
4. [LMB] **AVTIE DESKTOP**
5. [LMB] **AFRL/AFIT Joined-Wing DOE**
6. [MMB] **Delete Current**
7. [LMB] **Create New/Point Old**
8. [LMB] **Select Config File**
9. [LMB] desired file in Save Window Ex: baseline-configuration-v01.txt
10. [LMB] **Select Material File**
11. [LMB] desired file in Save Window Ex: aluminum-metric.txt
12. [LMB] **Select Mass File**
13. [LMB] desired file in Save Window Ex: baseline-weights-v01.txt
14. [LMB] **Read Config File**

15. [LMB] **Read Material File**

16. [LMB] **Read Mass File**

17. In window right of **Update Mission Leg**, enter Mission Leg integer (0, 1, or 2)

18. [LMB] **Update Mission Leg**

19. In window right of **Update Mission Leg Fraction**, enter Leg Fraction (Ex: 0.50)

20. [LMB] **Update Mission Leg Fraction**

21. Enter desired load factor into the box to the right of **Update Maneuver Load (NZ).**

22. [LMB] **Update Maneuver Load (NZ)**

23. [LMB] **Update AoA + Spread**

24. [LMB] **Update Twist + Spread**

25. [LMB] **Gen Stability Aero Table** (this will take approximately five minutes)

26. [LMB] **Update Weight Printout**

27. [LMB] **Trim Aero at Mass Ctr** (values in the third column to the right of **Update AoA + Spread** and **Update Twist + Spread** will change)

28. [MMB] **Update AoA + Spread**

29. [LMB] **Update AoA + Spread**

30. [MMB] **Update Twist + Spread**

31. [LMB] **Update Twist + Spread**

32. [LMB] **Gen PanAir Input**

33. [LMB] **Run PanAir**

34. [LMB] **Trim Aero at Mass Ctr** (values in the third column to the right of **Update AoA + Spread** and **Update Twist + Spread** will change)

35. Repeat Steps 28 – 34 until AoA and Twist values do not change.

36. Subtract the Jig Shape (Jig Shape is defined by the user) from the Twist angle.

37. Enter the new value into the box below **Update Flex Twist Angle**.

38. [LMB] **Update Flex Twist Angle**

39. Enter Jig Shape into the box to the right of **Update Twist + Spread**.

40. [LMB] **Update AoA + Spread**

41. [LMB] **Update Twist + Spread**

42. [LMB] **Gen NASTRAN Input**. This will generate a Linear Static NASTRAN model with the gravity and aerodynamic loads. Flexible twist will be enforced in the aft-wing.

AVTIE Flexible Trim Process

1. Open AML 3.3 from the desktop. [LMB] **OK**

2. [LMB] **My AML Utilities**

3. [LMB] **LOAD AVTIE**. Wait for AML Editor Window message: **AVTIE Loaded!**

4. [LMB] **AVTIE DESKTOP**

5. [LMB] **AFRL/AFIT Joined-Wing DOE**

6. [MMB] **Delete Current**

7. [LMB] **Create New/Point Old**

8. [LMB] **Select Config File**

9. [LMB] desired file in Save Window Ex: baseline-configuration-v01.txt

10. [LMB] **Select Material File**

11. [LMB] desired file in Save Window Ex: aluminum-metric.txt

12. [LMB] **Select Mass File**

13. [LMB] desired file in Save Window Ex: baseline-weights-v01.txt

14. [LMB] **Read Config File**

15. [LMB] **Read Material File**

16. [LMB] **Read Mass File**

17. In window right of **Update Mission Leg**, enter Mission Leg integer (0, 1, or 2)

18. [LMB] **Update Mission Leg**

19. In window right of **Update Mission Leg Fraction**, enter Leg Fraction (Ex: 0.50)

20. [LMB] **Update Mission Leg Fraction**

21. [LMB] **Increment FEM Analysis Step**

22. [LMB] **Read NASTRAN Disp**

23. [LMB] **Read NASTRAN Thick**

24. Steps 22 and 23 will read jw_displacement.punch and jw_thickness.punch

25. [LMB] **Update Weight Printout**

26. Enter **Wing Structure Mass** value into wing-mass-initial-guess variable in avo-joined-wing-right object.

27. [LMB] **Update Weight Printout**

28. Enter desired load factor into the box to the right of **Update Maneuver Load (NZ).**

29. [LMB] **Update Maneuver Load (NZ)**

30. [MMB] **Develop Flex Loads?**

31. [LMB] **Update AoA + Spread**

32. [LMB] **Update Twist + Spread**

33. [LMB] **Gen Stability Aero Table** (this will take approximately five minutes)

34. [LMB] **Update Weight Printout**

35. [LMB] **Trim Aero at Mass Ctr** (values in the third column to the right of **Update AoA + Spread** and **Update Twist + Spread** will change)

36. [MMB] **Update AoA + Spread**

37. [LMB] **Update AoA + Spread**

38. [MMB] **Update Twist + Spread**

39. [LMB] **Update Twist + Spread**

40. [LMB] **Gen PanAir Input**

41. [LMB] **Run PanAir**

42. [LMB] **Trim Aero at Mass Ctr** (values in the third column to the right of **Update AoA + Spread** and **Update Twist + Spread** will change)

43. Repeat Steps 36 – 42 until AoA and Twist values do not change.

44. Subtract the Jig Shape (Jig Shape is defined by the user) from the Twist angle.

45. Enter the new value into the box below **Update Flex Twist Angle**.

46. [LMB] **Update Flex Twist Angle**

47. Enter Jig Shape into the box to the right of **Update Twist + Spread**.

48. [LMB] **Update AoA + Spread**

49. [LMB] **Update Twist + Spread**

50. [LMB] **Gen NASTRAN Input**. This will generate a Linear Static NASTRAN model with the gravity and aerodynamic loads. Flexible twist will be enforced in the aft-wing.

Multiple Load Case Flexible Trim

Below is an alternate method when flexible trim is needed for several mission cases using the same thickness file.

1. Open AML 3.3 from the desktop. [LMB] **OK**

2. [LMB] **My AML Utilities**

3. [LMB] **LOAD AVTIE**. Wait for AML Editor Window message: **AVTIE Loaded!**

4. [LMB] **AVTIE DESKTOP**

5. [LMB] **AFRL/AFIT Joined-Wing DOE**

6. [MMB] **Delete Current**

7. [LMB] **Create New/Point Old**

8. [LMB] **Select Config File**

9. [LMB] desired file in Save Window Ex: baseline-configuration-v01.txt

10. [LMB] **Select Material File**

11. [LMB] desired file in Save Window Ex: aluminum-metric.txt

12. [LMB] **Select Mass File**

13. [LMB] desired file in Save Window Ex: baseline-weights-v01.txt

14. [LMB] **Read Config File**

15. [LMB] **Read Material File**

16. [LMB] **Read Mass File**

17. In window right of **Update Mission Leg**, enter Mission Leg integer (0, 1, or 2)

18. [LMB] **Update Mission Leg**

19. In window right of **Update Mission Leg Fraction**, enter Leg Fraction (Ex: 0.50)

20. [LMB] **Update Mission Leg Fraction**

21. Enter known **Wing Structure Mass** value into wing-mass-initial-guess variable in avo-joined-wing-right object.

22. [LMB] **Update Weight Printout**

23. Enter desired load factor into the box to the right of **Update Maneuver Load (NZ).**

24. [LMB] **Update Maneuver Load (NZ)**

25. [MMB] **Develop Flex Loads?**

26. [LMB] **Update AoA + Spread**

27. [LMB] **Update Twist + Spread**

28. [LMB] **Gen Stability Aero Table** (this will take approximately five minutes)

29. In AML Editor Window, enter the following line:

30. [LMB] **Step Through Analysis**

Develop Gust Loads

Below is the procedure to develop gust loads. Special care must be taken to ensure all steps are followed in the exact order listed here.

1. Open AML 3.3 from the desktop. [LMB] **OK**

2. [LMB] **My AML Utilities**

3. [LMB] **LOAD AVTIE**. Wait for AML Editor Window message: **AVTIE Loaded!**

4. [LMB] **AVTIE DESKTOP**

5. [LMB] **AFRL/AFIT Joined-Wing DOE**

6. [MMB] **Delete Current**

7. [LMB] **Create New/Point Old**

8. [LMB] **Select Config File**

9. [LMB] desired file in Save Window Ex: baseline-configuration-v01.txt

10. [LMB] **Select Material File**

11. [LMB] desired file in Save Window Ex: aluminum-metric.txt

12. [LMB] **Select Mass File**

13. [LMB] desired file in Save Window Ex: baseline-weights-v01.txt

14. [LMB] **Read Config File**

15. [LMB] **Read Material File**

16. [LMB] **Read Mass File**

17. In window right of **Update Mission Leg**, enter Mission Leg integer (0, 1, or 2)

18. [LMB] **Update Mission Leg**

19. In window right of **Update Mission Leg Fraction**, enter Leg Fraction (Ex: 0.50)

20. [LMB] **Update Mission Leg Fraction**

21. Enter desired load factor into the box to the right of **Update Maneuver Load (NZ)**.

22. [LMB] **Update Maneuver Load (NZ)**

23. Enter known **Wing Structure Mass** value into wing-mass-initial-guess variable in avo-joined-wing-right object.

24. Enter known dynamic pressure value into dynamic-pressure variable in avo-joined-wing-right object.

25. [LMB] **Update Weight Printout**

26. [LMB] **Increment FEM Analysis Step**

27. If jw_displacement.punch file available, [LMB] **Read NASTRAN Disp**

28. If jw_thickness.punch file available, [LMB] **Read NASTRAN Thick**

29. [LMB] **Update Weight Printout**

30. If step 27 was executed, [MMB] **Develop Flex Loads?**

31. [LMB] **Gen Stability Aero Table** (this will take approximately five minutes)

32. [LMB] **Update Weight Printout**

33. [LMB] **Trim Aero at Mass Ctr** (values in the third column to the right of **Update AoA + Spread** and **Update Twist + Spread** will change)

34. [MMB] **Update AoA + Spread**

35. [LMB] **Update AoA + Spread**

36. [MMB] **Update Twist + Spread**

37. [LMB] **Update Twist + Spread**

38. [LMB] **Gen PanAir Input**

39. [LMB] **Run PanAir**

40. [LMB] **Trim Aero at Mass Ctr** (values in the third column to the right of **Update AoA + Spread** and **Update Twist + Spread** will change)

41. Repeat Steps 34 – 40 until AoA and Twist values do not change.

42. Subtract the Jig Shape (Jig Shape is defined by the user) from the Twist angle.

43. Enter the new value into the box below **Update Flex Twist Angle**.

44. [LMB] **Update Flex Twist Angle**

45. Enter Jig Shape into the box to the right of **Update Twist + Spread**.

46. [LMB] **Update AoA + Spread**

47. [LMB] **Update Twist + Spread**

48. [LMB] **Gen NASTRAN Input**. This will generate a Linear Static NASTRAN model with the gravity and aerodynamic loads. Flexible twist will be enforced in the aft-wing.

49. Transfer NASTRAN file to folder containing **gusttrim1g.m** file and **mpfsdelement.pch** file.

50. Start MATLAB

51. Execute **gusttrim1g.m**. This will create a jw_displacement.punch file

52. Transfer the jw_displacement.punch to the AVTIE/…/av-astros-data directory

53. [LMB] **Increment FEM Analysis Step**

54. [LMB] **Read NASTRAN Disp**

55. [LMB] **Read NASTRAN Thick**

56. [LMB] **Update Weight Printout**

57. [MMB] **Develop Flex Loads?**

58. [LMB] **Gen Stability Aero Table** (this will take approximately five minutes)

59. [LMB] **Update Weight Printout**

60. [LMB] **Trim Aero at Mass Ctr** (values in the third column to the right of **Update AoA + Spread** and **Update Twist + Spread** will change)

61. [MMB] **Update AoA + Spread**

62. [LMB] **Update AoA + Spread**

63. [MMB] **Update Twist + Spread**

64. [LMB] **Update Twist + Spread**

65. [LMB] **Gen PanAir Input**

66. [LMB] **Run PanAir**

67. [LMB] **Trim Aero at Mass Ctr** (values in the third column to the right of **Update AoA + Spread** and **Update Twist + Spread** will change)

68. Repeat Steps 60 – 67 until AoA and Twist values do not change.

69. Add the ?a value calculated from equation 3-4 to the angle of attack.

70. [MMB] **Update AoA + Spread**

71. [LMB] **Gen PanAir Input**

72. [LMB] **Run PanAir**

73. CAUTION: Do NOT **Trim Aero at Mass Ctr** at this point!

74. Subtract the Jig Shape (Jig Shape is defined by the user) from the Twist angle.

75. Enter the new value into the box below **Update Flex Twist Angle**.

76. [LMB] **Update Flex Twist Angle**

77. Enter Jig Shape into the box to the right of **Update Twist + Spread**.

78. [LMB] **Update AoA + Spread**

79. [LMB] **Update Twist + Spread**

80. [LMB] **Gen NASTRAN Input**. This will generate a Linear Static NASTRAN model with the gravity and gust aerodynamic loads. Flexible twist will be enforced in the aft-wing.

Appendix C:
Additional Results

The gust loads were initially added to the linear optimized and trimmed aluminum model (Table C-1).

Iteration	Wing Structure (kg)	Gross Take-Off (kg)
7	6250	38504
8	6219	38474

Table C-1. Optimized Mass at Linear Structural Iterations, Including Gust Loads

Including the critical gust load conditions increased the optimized mass approximately 2400 kg. However, in this instance, the model was trimmed to a 1G flight condition using the deformations created by the gust condition. This produced incorrect aerodynamic loads, but still converged to a minimum weight design. Again, the fuel requirement was not recalculated.

Table C-2 lists the final optimized trim conditions using non-linear analysis. These aerodynamic conditions were developed through AVTIE flexible trim.

Mission Leg and Fraction	Aerodynamic Load Factor	Angle of Attack	Aft-Wing Twist
0.00	2.5G	10.68	7.72
0.50	2.5G	9.12	7.43
1.00	2.5G	21.02	13.6
1.50	2.5G	14.23	13.3
2.00	2.5G	1.29	5.44
2.50	2.5G	0.62	5.24
2.98	2.5G	-0.02	5.06
2.98	3.34G	0.29	-0.70
2.98	3.42G	1.57	-0.10

Table C-2. Final Aerodynamic Trim Conditions, All Flight Loads

Bibliography

1. Gallman, J.W., and Kroo, I.M., "Structural Optimization for Joined-Wing Synthesis", *Journal of Aircraft*, Vol. 33, No. 1, January-February 1996, pp. 214-223.

2. Moorhouse, D., and others. "Sensorcraft – Phase I," Air Vehicles technology assessment, March 2000.

3. "Adaptive Modeling Language Basic Training Manual: Version 2.07," TechnoSoft Incorporated, 2001.

4. Blair, M., and Canfield, R., "A Joined-Wing Structural Weight Modeling Study", AIAA-2002-1337, presented at the 43rd AIAA/ASME/ASCE/AHS/ASC Structures, Structural Dynamics and Materials Conference, Denver, CO, 22-25 April 2002.

5. " MATLAB Student Version, Release 12", The Math Works, Inc., 2001.

6. "MSC.NASTRAN Version 68 Reference Manual", MacNeal-Schwendler Corporation, 1995.

7. "User's Guide-PAN AIR Technology Program for Solving Potential Flow about Arbitrary Configurations," Public Domain Aeronautical Software, 1992.

8. Northrop Grumman Corporation, "SensorCraft Low Band Conformal Load Bearing Antenna Structures (S-CLAS): R & D Status Report No. 13", Contract No. F33615-00-D-3054, 29 August 2002.

9. Schwartz, J., Canfield, R., and Blair, M., "Aero-Structural Coupling and Sensitivity of a Joined-Wing SensorCraft", submitted for presentation at the 44th AIAA/ASME/ASCE/AHS/ASC Structures, Structural Dynamics and Materials Conference, April 2003.

10. Wolkovich, J., "The Joined Wing: An Overview," *Journal of Aircraft*, Vol. 23, No. 3, 1986, pp. 161-178.

11. Wolkovich, J., Joined Wing Aircraft, U.S. Patent 3,942,747, March 1976.

12. Samuels, M. F., "Structural Weight Comparison of a Joined Wing and a Conventional Wing," *Journal of Aircraft*, Vol. 19, No. 6, 1982, pp. 485-491.

13. Sager, Garrett L. President, Sager Aerospace Inc., San Antonio, TX. Telephone interview. 18 August 2002.

14. Smith, S.C., Cliff, S.E., and Kroo, I.M., "The Design of a Joined-Wing Flight Demonstrator Aircraft", AIAA Paper 87-2930, AIAA/AHS/ASEE Aircraft Design, Systems and Operations Meeting, St. Louis, MO, 14-16 September 1987.

15. Lin, H-H., Jhou, J., and Stearman, R., "Influence of Joint Fixiti on the Aeroelastic Characteristics of a Joined Wing Structure", AIAA Paper 90-0980, Proceedings of the 31st AIAA/ASME/ASCE/AHS/ASC Structures, Structural Dynamics and Materials Conference, Long Beach, CA, April 1990, pp. 1442-1454.

16. Kroo, I. M., Gallman, J. W., and Smith, S. C., "Aerodynamic and Structural Studies of Joined-Wing Aircraft," *Journal of Aircraft*, Vol. 28, No. 1, January-February 1991, pp. 74-81.

17. Gallman, J.W., Smith, S.E., and Kroo, I.M., "Optimization of Joined-Wing Aircraft", *Journal of Aircraft*, Vol. 30, No. 6, November-December 1993, pp. 897-905.

18. Livne, E., "Aeroelasticity of Joined-Wing Airplane Configurations: Past Work and Future Challenges – A Survey", AIAA-2001-1370, presented at the 42nd AIAA/ASME/ASCE/AHS/ASC Structures, Structural Dynamics and Materials Conference, Seattle, WA, 16-19 April 2001.

19. Canfield, R., Ghanem, R., and Petit, C., "Stochastic Analysis of an Aeroelastic System", presented at the 15th ASCE Engineering Mechanics Conference, Columbia University, New York, NY, 2-5 June 2002.

20. Lan, Chuan-Tau E. and Roskam J. *Airplane Aerodynamics and Performance* (2nd Edition). Ottawa: Roskam Aviation and Engineering Corporation, 1988.

21. Schwartz, J., Canfield, R., and Blair, M., "Aero-Structural Coupling and Sensitivity of a Joined-Wing SensorCraft", submitted for presentation at the 44th AIAA/ASME/ASCE/AHS/ASC Structures, Structural Dynamics and Materials Conference, April 2003.

22. Raymer, Daniel P. *Aircraft Design: A Conceptual Approach* (2nd Edition). Washington DC: American Institute of Aeronautics and Astronautics, Inc., 1992.

23. Cook, Robert D., et al., Concepts and Applications of Finite Element Analysis, Fourth Edition, University of Wisconsion-Madison, 2002.

24. Lee, John M., *MSC.NASTRAN Version 69+ Linear Static Analysis User's Guide*. MacNeal-Schwendler Corporation, 1995.

25. Lee, Sang H., *MSC.NASTRAN Handbook for Nonlinear Analysis Version 67*. MacNeal-Schwendler Corporation, 1992.

26. Department of Defense. *Metallic Materials and Elements for Aerospace Vehicle Structures*. MIL-HDBK-5H. Washington: GPO, 1 December 1998.

27. Choi, Seung-Kyum, Grandhi, Ramana V., et al, "Polynomial Chaos Expansion with Latin Hypercube Sampling for Predicting Response Variability", AIAA-2003-8527, 2003.

Vita

Captain Ronald W. Roberts, Jr. graduated from Mills E. Godwin High School in Richmond, Virginia. He entered undergraduate studies at Embry-Riddle Aeronautical University in Daytona Beach, Florida where he graduated with a Bachelor of Science degree in Aerospace Engineering in December 1993. He enlisted in September 1994 and was stationed at Dover AFB, Delaware as a C-5 aircraft maintenance technician.

He entered Officer Training School in January 1998 and was commissioned in April 1998. His next assignment was at Schriever AFB as an engineer for the 1st Space Operations Squadron. In August 2001, he entered the Graduate School of Engineering and Management, Air Force Institute of Technology.

REPORT DOCUMENTATION PAGE

Form Approved
OMB No. 074-0188

1. REPORT DATE *(DD-MM-YYYY)*	2. REPORT TYPE	3. DATES COVERED *(From – To)*
10-03-2003	**Master's Thesis**	Sept 2001 – Mar 2003

4. TITLE AND SUBTITLE

SENSOR-CRAFT ANALYTICAL CERTIFICATION

5a. CONTRACT NUMBER

5b. GRANT NUMBER

5c. PROGRAM ELEMENT NUMBER

6. AUTHOR(S)

Roberts, Ronald W. Jr., Captain, USAF

5d. PROJECT NUMBER

5e. TASK NUMBER

5f. WORK UNIT NUMBER

7. PERFORMING ORGANIZATION NAMES(S) AND ADDRESS(S)

Air Force Institute of Technology
Graduate School of Engineering and Management (AFIT/ENY)
2950 HOBSON WAY
WRIGHT PATTERSON AFB OH 45433-7765

8. PERFORMING ORGANIZATION REPORT NUMBER

AFIT/GAE/ENY/03-6

9. SPONSORING/MONITORING AGENCY NAME(S) AND ADDRESS(ES)

AFRL/VASD
2210 Eighth St. Rm 220
Wright Patterson AFB, OH 45433
937-255-8430
Dr. Maxwell Blair

DAGSI
3155 Research Blvd. Ste 205
Kettering, OH 45420
937-781-4000
Dr. Elizabeth Downie

10. SPONSOR/MONITOR'S ACRONYM(S)

11. SPONSOR/MONITOR'S REPORT NUMBER(S)

12. DISTRIBUTION/AVAILABILITY STATEMENT

APPROVED FOR PUBLIC RELEASE; DISTRIBUTION UNLIMITED

13. SUPPLEMENTARY NOTES

14. ABSTRACT

This study developed a multi-disciplinary conceptual design of a joined-wing sensor-craft. Initial analysis was conducted using an aluminum model. Linear fully stressed design and flexible aerodynamic trim were used to converge to a minimum weight design that was aerodynamically stable. This optimized design was buckling safe. A similar optimization process using non-linear fully stressed design and flexible aerodynamic trim was conducted. The non-linear structural deformation was over ten times greater than the linear structural deformation. Again, the model was structurally and aerodynamically optimized. The linear optimization was repeated using a composite structural model incorporating Conformal Load-bearing Antenna Structures. This research demonstrated the importance of considering non-linearity and the coupling of aerodynamic and structural design.

15. SUBJECT TERMS

Sensor-Craft, Joined-Wing, Fully Stressed Design, Non-Linear Analysis, Air Vehicles Technology Integration Environment (AVTIE)

16. SECURITY CLASSIFICATION OF:			17. LIMITATION OF ABSTRACT	18. NUMBER OF PAGES	19a. NAME OF RESPONSIBLE PERSON
a. REPORT	b. ABSTRACT	c. THIS PAGE			Robert A. Canfield, LtCol
U	U	U	UU	110	19b. TELEPHONE NUMBER *(Include area code)* (937) 255-6565, ext 4641; e-mail: robert.canfield@afit.edu

Standard Form 298 (Rev. 8-98)
Prescribed by ANSI Std. Z39-18